High-spin structure, K isomers, and state mixing in the neutron-rich isotopes ^{173}Tm and ^{175}Tm

R. O. Hughes, G. J. Lane, G. D. Dracoulis, A. P. Byrne, P. H. Nieminen, H. Watanabe, M. P. Carpenter, P. Chowdhury, R. V. F. Janssens, F. G. Kondev, T. Lauritsen, D. Seweryniak, and S. Zhu

Phys. Rev. C **86**, 054314 — Published 26 November 2012

DOI: 10.1103/PhysRevC.86.054314

High-spin structure, K isomers and state mixing in the neutron-rich isotopes ^{173}Tm and ^{175}Tm.

R. O. Hughes,[1,*] G. J. Lane,[1] G. D. Dracoulis,[1] A. P. Byrne,[1]
P. H. Nieminen,[1,†] H. Watanabe,[1,‡] M. P. Carpenter,[2] P. Chowdhury,[3]
R. V. F. Janssens,[2] F. G. Kondev,[4] T. Lauritsen,[2] D. Seweryniak,[2] and S. Zhu[2]

[1]*Department of Nuclear Physics, Research School of Physics and Engineering, Australian National University, Canberra, A.C.T. Australia 0200*

[2]*Physics Division, Argonne National Laboratory, Argonne IL 60439, USA*

[3]*Department of Physics, University of Massachusetts, Lowell, MA 01854, USA*

[4]*Nuclear Engineering Division, Argonne National Laboratory, Argonne IL 60439, USA*

Abstract

High-spin states in the odd-proton thulium isotopes ^{173}Tm and ^{175}Tm have been studied using deep-inelastic reactions and γ-ray spectroscopy. In ^{173}Tm, the low-lying structure has been confirmed and numerous new states have been identified, including a three-quasiparticle, $K^\pi = 19/2^-$ isomer with a lifetime of $\tau = 360(100)$ ns at 1906 keV and a five-quasiparticle $K^\pi = 35/2^-$ isomer with a lifetime of $\tau = 175(40)$ ns at 4048 keV. The $K^\pi = 35/2^-$ state is interpreted as a t-band configuration that shows anomalously fast decays. In ^{175}Tm, the low-lying structure has been re-evaluated, a candidate state for the $9/2^-[514]$ orbital has been identified at 1175 keV, and the $7/2^-[523]$ bandhead has been measured to have a lifetime of $\tau = 460(50)$ ns. Newly identified high-K structures in ^{175}Tm include a $K^\pi = 15/2^-$ isomer with a lifetime of $\tau = 64(3)$ ns at 947 keV, and a $K^\pi = 23/2^+$ isomer with a lifetime of $\tau = 30(20)$ μs at 1518 keV. The $K^\pi = 15/2^-$ isomer shows relatively enhanced decays to the $7/2^-[523]$ band that can be explained by chance mixing with the $15/2^-$ member of the $7/2^-$ band. Multi-quasiparticle calculations have been performed for ^{173}Tm and ^{175}Tm, the results of which compare well with the experimentally observed high-spin states.

PACS numbers: 21.10.Re, 21.10.Tg, 23.20.Lv, 27.70.+q

*Electronic address: rhughes2@richmond.edu; Present address, Dept of Physics, University of Richmond, 28 Westhampton Way, Richmond, VA 23173, USA

†Present address, Dept of Physics, University of Jyväskylä, P.O. BOX 35, FI-40014 Jyväskylä, Finland

‡Present address, Nuclear Physics Research Division, RIKEN Nishina Center for Accelerator-based Science, 2-1 Hirosawa, Wako, Saitama, Japan 351-0198

I. INTRODUCTION

The rare-earth nuclei around mass ~ 180 are quadrupole deformed and typically have orbitals with large spin projection on the symmetry axis, Ω, near both the proton and neutron Fermi surfaces. This leads to the prospect of multi-quasiparticle states with high K (where $K = \sum \Omega_i$) occurring near the yrast line. K isomers are consequently expected in this region. These arise when a state can only decay via transitions of multipolarity, L, that violate the K selection rule by an order of forbiddenness, $\nu = \Delta K - L$.

The present work is part of an ongoing effort to map isomerism in the neutron-rich, deformed nuclei using deep-inelastic reactions. This has so far encompassed studies of various isotopes of tungsten, tantalum, hafnium, lutetium, ytterbium and erbium (see e.g. [1–7], and references therein). Deep-inelastic reactions have become a key tool in studying neutron-rich rare-earth nuclei, since they cannot be populated by more conventional reactions.

While a substantial number of the nuclei in the mass-180 region have been studied, there are still gaps in the experimental data available, particularly when moving away from stability to very neutron-rich isotopes. For the thulium isotopes (Z = 69), beyond the stable isotope ^{169}Tm, recent work in ^{171}Tm revealed the structure of a three-quasiparticle, $19/2^+$ isomer [8, 9], while in ^{172}Tm a low-lying, two-quasiparticle, $K^\pi = 6^+$ isomer was found in incomplete fusion studies [10]. Nevertheless, the nuclear structure information for isotopes beyond ^{171}Tm is limited to relatively low spins and to one- or two-quasiparticle states for odd-even and odd-odd isotopes, respectively. The odd-A isotopes ^{173}Tm and ^{175}Tm are the focus of the present work. The proton Fermi surface lies closest to the $1/2^+[411]$ Nilsson orbital, with nearby $7/2^-[523]$ and $7/2^+[404]$ states. The neutron Fermi surface is near the $5/2^-[512]$, $7/2^-[514]$, $7/2^+[633]$ and $9/2^+[624]$ orbitals. Combinations of these orbitals should lead to low-lying, high-K, multi-quasiparticle states.

II. EXPERIMENTAL PROCEDURES

The experiments were performed at Argonne National Laboratory using ^{176}Yb (97% enriched), ^{176}Lu (47% enriched), ^{174}Yb (95% enriched) and ^{175}Lu (nat. - 97% ^{175}Lu, 3% ^{176}Lu) targets and an 820-MeV ^{136}Xe beam. The beam energy and target thicknesses of about 6 mg/cm^2 were chosen to maximize the yields of deep inelastic and transfer reactions,

by integrating energies from ∼24 % above the Coulomb barrier down to the barrier, due to the energy loss in the target. The reaction products were stopped in gold backings. The comparatively light beam (other studies used a ^{238}U beam [11]) was chosen to reduce the background from strong Coulomb excitation while still producing large spin and mass transfer. Gammasphere consisted of 101 Compton suppressed germanium detectors in the various experiments.

The majority of data collection was performed with a pulsed beam, using nanosecond pulses and 825 ns intervals. The coincidence events were collected with a coincidence overlap of approximately ±800 ns. About 3×10^9, 2×10^9, 2×10^8 and 2×10^8 coincidence events of three or higher fold were collected for the ^{176}Yb, ^{176}Lu, ^{174}Yb and ^{175}Lu targets, respectively. Data were also collected with a dual coincidence requirement and chopping conditions designed to measure long isomer lifetimes. For the ^{176}Lu target, on/off chopping regimes of 10/40 μs, 20/60 μs, 100/300 μs and 1/3 ms were used, while for the ^{176}Yb target, only one chopping regime with 1/3 ms was used.

III. ANALYSIS TECHNIQUES

The γ-ray data were initially presorted into the Blue database [12], including gain corrections, time corrections and the removal of detectors with poor timing or energy resolution. The data were subsequently sorted into in-beam (−30 ns to +100 ns) and out-of-beam (+100 ns to +750 ns) γ-γ-γ coincidence cubes for analysis with the Radware [13] software package. Asymmetric histograms, such as γ-γ-time-difference and γ-γ-clock cubes utilized for measuring lifetimes were analyzed using software built on the core program Root [14]. The thulium isotopes were most strongly observed with the ^{176}Yb target, and the majority of coincidence analyses was conducted using these data sets.

A. Gammasphere Efficiency

The initial relative efficiency measurement for the present study used ^{152}Eu, ^{182}Ta and ^{241}Am source data collected in singles mode. However, it was observed that the relative efficiency of low-energy γ rays gave measured intensities in the γ-γ-γ cube which were lower than expected, possibly due partially to the lower fold of cascades measured from the sources

compared to in-beam data. In addition, the time-constraints placed on the coincidence cube can suppress low-energy transitions due to time-walk. Additional internal calibrations were performed to evaluate the efficiency for low-energy lines using various delayed cascades measured below known isomers in the γ-γ-γ coincidence cubes. However, the limited number of available points results in a large uncertainty at low energies ($\sim$30% below 60 keV).

B. Internal Conversion and Transition Multipolarities

Total conversion coefficients were extracted (using appropriate gating conditions in γ-γ-γ cubes) by balancing the intensities of transitions in decay paths where at least one γ ray has a known multipolarity. In a number of cases, comparison of these with theoretical predictions [15] allowed transition multipolarities to be either deduced or constrained.

C. Isotopic Assignments

In deep-inelastic and binary or few-nucleon transfer reactions, the beam-like and target-like products are mass correlated, since the total mass of the beam and target must equal the sum over the reaction products. As an example, for the ^{136}Xe beam on a ^{176}Yb target, a target-like fragment of ^{175}Tm will be correlated with a beam-like fragment of ^{137}Cs. As a result, prompt γ rays from ^{137}Cs and ^{175}Tm should be in coincidence with each other, following a proton-transfer reaction. However, it is also common for particle-evaporation from the beam-like and target-like reaction products to follow the primary reaction. Broda *et al.* [16, 17] found that, typically, a few nucleons are lost, generally neutrons, so that the coincident beam-like and target-like reaction products are not necessarily specified uniquely. The production of thulium isotopes lighter than ^{175}Tm (in the ^{176}Yb target dataset, used for the majority of analysis) seemed to proceed predominantly via the initial production of ^{137}Cs and ^{175}Tm, followed by the evaporation of neutrons from ^{175}Tm. This was evident from the fact that γ rays associated with ^{137}Cs were observed in coincidence with all of the thulium structures identified in the prompt data.

The systematic nature of the present series of experiments (the use of different targets with the same experimental conditions) has made it possible to observe the population cross-sections of various nuclei depending on their proximity to the target isotope. The relative

yields from different targets can, in some cases, be used to guide isotopic assignments. Structures associated with ^{175}Tm, for example, were very weakly observed with targets other than ^{176}Yb. This is expected since ^{175}Tm is only one proton removed from ^{176}Yb, whereas more complex proton and neutron transfers are required to produce ^{175}Tm from ^{174}Yb, ^{175}Lu and ^{176}Lu.

The relative population intensities of different structures assigned to thulium were obtained by measuring the γ-ray intensities of transitions associated with each structure using double-gated coincidence spectra from the triples data of all four target datasets. Table I presents these relative population intensities labelled in each case with the gating transitions. The yields were normalized to take into account the different integrated beam in each case. The various structures are grouped by the thulium isotope to which they are assigned (structures associated with ^{172}Tm and ^{174}Tm will be discussed elsewhere [18]). The population intensities of structures belonging to ^{174}Tm and ^{175}Tm rapidly fall off for the ^{174}Yb, ^{175}Lu and ^{176}Lu target data relative to the ^{176}Yb target dataset. Note also the high population intensity for ^{171}Tm with the ^{175}Lu target (the α-transfer channel). In the case of the ^{176}Lu target, the large ^{175}Lu component as well as significant thorium contamination may make the ratios unreliable. (The latter contamination is linked to the use of thorium in the reduction process involved in target production.) The relative population intensity information was important for isotopic assignments in the present study, since little previous spectroscopic information was available.

IV. RESULTS

A. ^{175}Tm

Figure 1 presents out-of-beam γ-ray spectra associated with ^{175}Tm. The present level scheme (Fig. 2) is consistent with the previous assignments of Løvhøiden *et al.* [19] for the low-lying members of the $1/2^+[411]$ and $7/2^-[523]$ bands. (Note that Ref. [19] used charged-particle studies resulting in 2-4-keV uncertainties in level energies.)

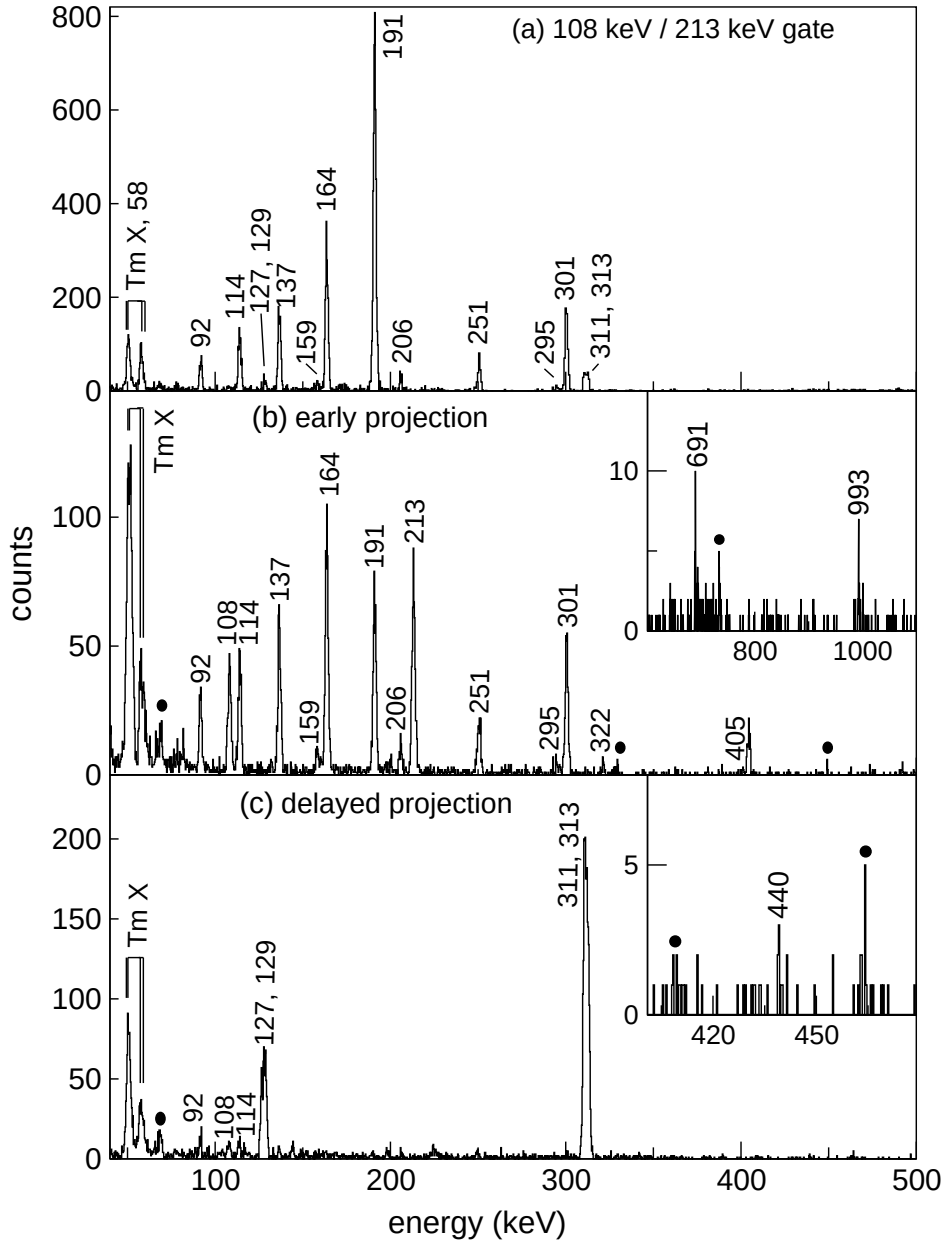

FIG. 1: Gamma-ray spectra for ^{175}Tm. (a): Spectrum obtained with a double gate on the 108/213-keV γ rays. (b): Spectrum produced in a sum of 127/313- and 129/311-keV double gates projecting 80-800 ns early in time. The inset provides an expanded view of the higher energy region. (c) Spectrum resulting from a sum of 164/(108,114,137,191,213)-keV, and 301/(108,114,191,213)-keV double gates, projecting 80-800 ns early in time with respect to the gating transitions. Low-energy time walk means that the 92-, 108- and 114-keV transitions from above the isomer are seen weakly in the spectrum. The inset shows an expanded view around the (weak) 440-keV transition. Contaminants are labelled with filled circles.

TABLE I: Relative population intensities of thulium structures in the ^{176}Yb, ^{174}Yb, ^{176}Lu and ^{175}Lu data sets normalized to the ^{176}Yb data point.

Isotopic	Signature	Target			
assignment	γ rays (keV)	$^{176}_{70}$Yb$_{106}$	$^{174}_{70}$Yb$_{104}$	$^{176}_{71}$Lu$_{105}$	$^{175}_{71}$Lu$_{104}$
$^{171}_{69}$Tm$_{102}$	352/428	1.0(1)	1.5(3)	0.7(1)	3.5(3)
$^{172}_{69}$Tm$_{103}$	224/846	1.0(1)	1.3(3)	0.5(1)	0.9(2)
	102/228	1.0(1)	0.9(2)	0.4(2)	0.6(3)
$^{173}_{69}$Tm$_{104}$	152/171	1.0(1)	1.1(2)	0.4(1)	0.5(1)
	154/166	1.0(1)	1.0(2)	0.4(1)	0.4(1)
	548/704	1.0(1)	0.7(2)	0.3(1)	0.3(2)
$^{174}_{69}$Tm$_{105}$	359/438	1.0(1)	0.5(3)	0.1(1)	0.1(1)
	200/489	1.0(1)	0.3(1)	0.1(1)	0.1(1)
$^{175}_{69}$Tm$_{106}$	108/213	1.0(1)	0.1(1)	<0.1	<0.1

[a]The yields deduced for ^{176}Lu may be unreliable due to high ^{175}Lu content (∼53%), and thorium contamination in the target.

1. *1/2$^+$[411], ground state band*

The ground state rotational band was previously assigned up to the $9/2^+$ member by Løvhøiden *et al.* [19], albeit with large uncertainties in the level energies, which prevented differentiation between the $7/2^+$ and $5/2^+$ levels, for example. In the present work, the band has been extended to the $23/2^+$ member utilizing the in-beam gated γ-γ-γ coincidence cube from the ^{176}Yb target data. It should be noted that the Doppler broadening evident, for example, in the spectra of Fig. 3, limits the observation of higher-spin rotational states that are not fed by isomers.

Figure 3(a) displays the $E2$ crossover transitions in the $3/2^+$, $7/2^+$, $11/2^+$... sequence (signature, $\alpha = -1/2$). The low-lying members of the weaker $1/2^+$, $5/2^+$, $9/2^+$... sequence (signature, $\alpha = +1/2$) are observed in the out-of-beam data since the $9/2^+$ state is populated by an 87-keV branch from the $7/2^-$ isomer. Higher-lying transitions associated with the

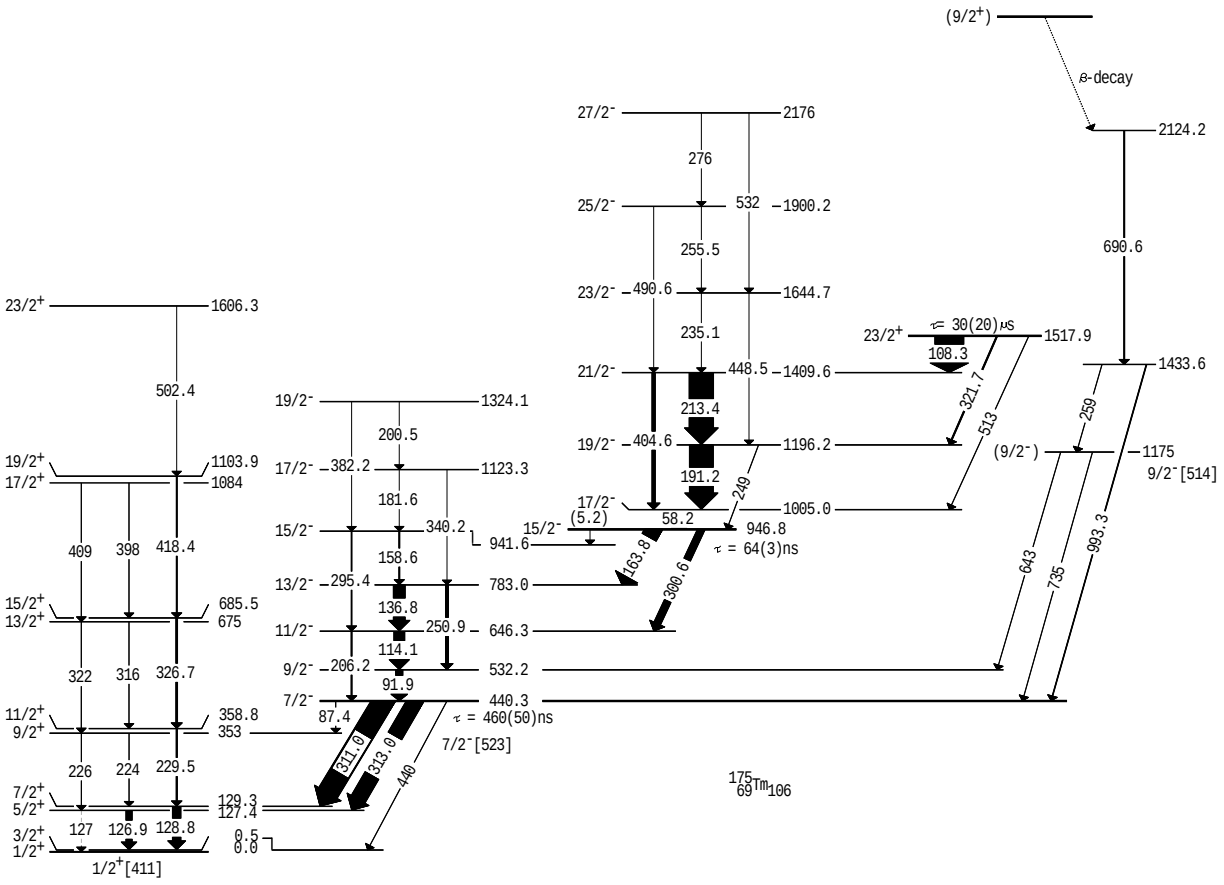

FIG. 2: Proposed level scheme for ^{175}Tm. Arrow widths are proportional to the relative γ-ray intensities. The state at 2124 keV is proposed to be populated via β decay from the $(9/2^+)$ ground state of ^{175}Er.

$\alpha = +1/2$ signature band are seen weakly in the in-beam spectra of Figs. 3(a), (b) and (c).

Figure 4 plots the rotational energy constant for the two signature sequences of the $1/2^+[411]$ bands of ^{171}Tm [20], ^{173}Tm and ^{175}Tm. The plots for ^{171}Tm and ^{175}Tm are very similar, supporting the present assignments. (The ^{173}Tm results are limited to low spin). The energy for the $J^\pi = 3/2^+$ level in ^{175}Tm is estimated at $E_x = 0.5(4)$ keV by the extrapolation shown in the figure. The inferred 127(1)-keV, $5/2^+ \rightarrow 1/2^+$ transition would, therefore, be unresolved from the stronger 126.9(3)-keV, $5/2^+ \rightarrow 3/2^+$ transition in Fig. 1 (c), for example. The results for the $1/2^+[411]$ band in ^{175}Tm disagree with those of Zhang *et al.* [21]. However, the present, more comprehensive results are internally consistent, in agreement with systematics, and also with the results of Løvhøiden *et al.* [19].

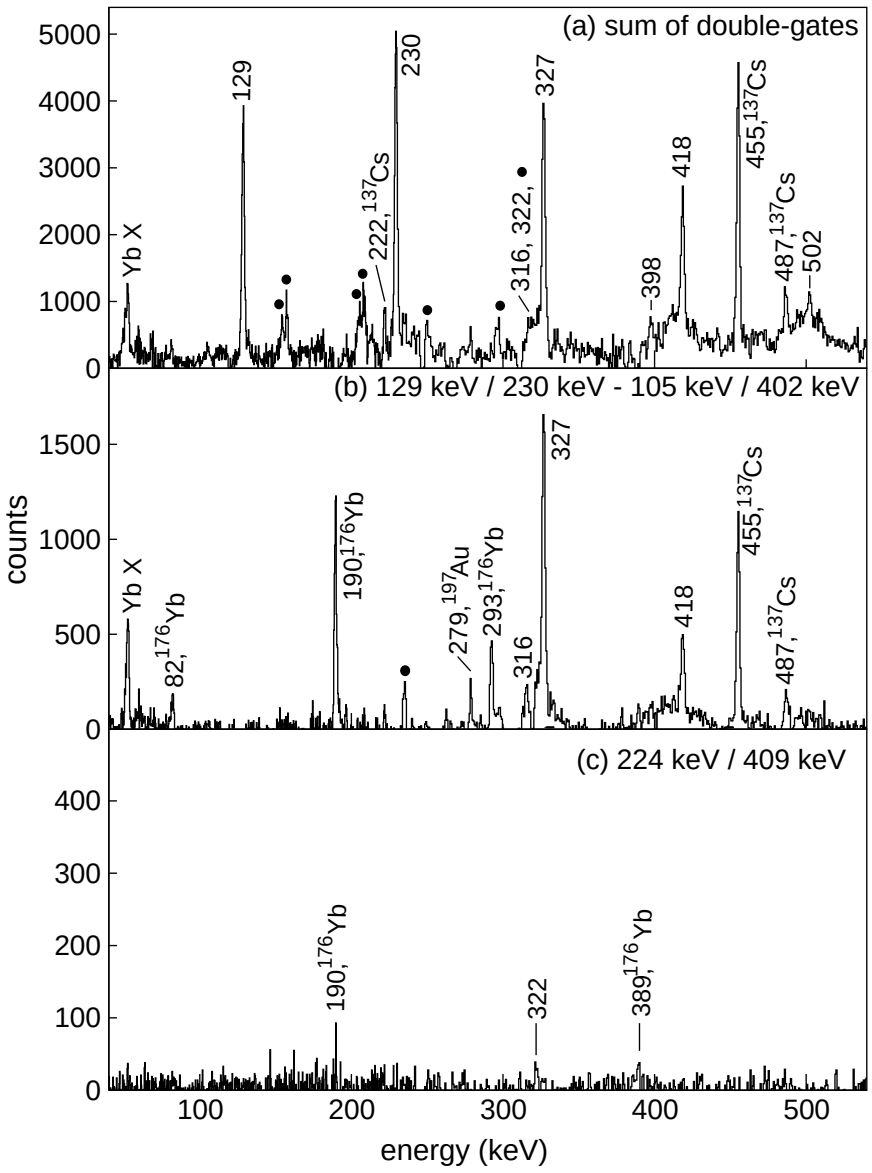

FIG. 3: In-beam γ-ray spectra associated with the ground state band in ^{175}Tm. Identified contaminants are labelled with filled circles. Higher-energy transitions display significant Doppler broadening. (a): Spectrum produced with a sum of in-beam 129/230-, 129/327-, 129/418-, 230/327-, 230/418- and 327/418-keV double coincidence gates. Cross-coincidences with ^{137}Cs imply a thulium isotope with mass 171$\leq$A$\leq$175. (b): Spectrum obtained with a 129/230-keV double gate. The 105/402-keV double gate has been subtracted to eliminate some contaminant lines. (c): Spectrum resulting from a 224/409-keV double gate, showing the 322-keV line.

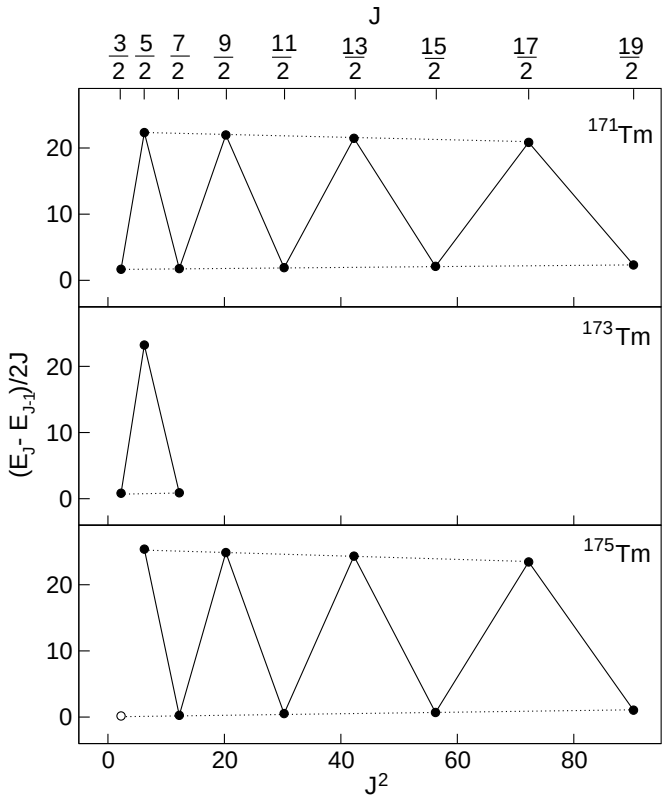

FIG. 4: Plots of the rotational energy constant for the two signature sequences in the $1/2^+[411]$ bands of ^{171}Tm [20], ^{173}Tm and ^{175}Tm. The open circle in the ^{175}Tm plot is an extrapolation used to extract the $3/2^+$ level energy.

2. 7/2⁻[523] isomer at 440 keV

A $7/2^-[523]$ configuration assignment was proposed for this state by Løvhøiden *et al.* [19], but no lifetime was reported. A time-difference spectrum produced from a sum of double coincidence gates placed below and above the isomer from which a lifetime of $\tau = 460(50)$ ns was deduced is presented in Fig. 5.

Extensions of the $7/2^-[523]$ rotational band up to its $19/2^-$ member were obtained by analyzing a matrix produced with a requirement that coincidence events occurred both in-beam, and also 30-800 ns earlier than the 311- or 313-keV transitions.

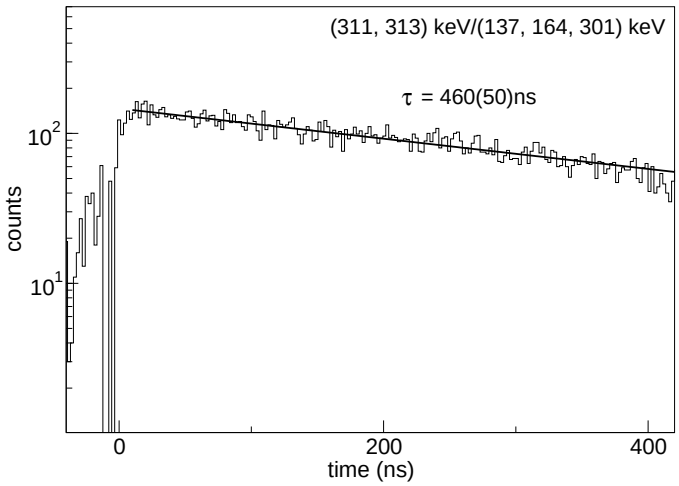

FIG. 5: Time-difference spectrum produced from transitions above and below the $7/2^-[523]$ isomer at 440 keV.

3. Levels at 1175, 1434 and 2124 keV

The 691- and 993-keV γ rays that are observed above the $7/2^-$ isomer in Fig. 1(b), display a constant intensity over the full out-of-beam time range of the 1 ms/3 ms chopped data, implying a feeding lifetime of the order of several milliseconds or longer. The associated states also feed into a $K = 7/2$ level with no other obvious decay branches, suggesting low-K assignments for the 1434- and 2124-keV levels. These states are presumed therefore to be populated by feeding from the β decay of the $(9/2^+)$ ground state of ^{175}Er [22]. A third level was also identified at 1175 keV, exhibiting weak 643- and 735-keV decay branches to the $7/2^-$ and $9/2^-$ members of the $7/2^-[523]$ band. Comparison with the 1213-keV, $9/2^-[514]$ state in ^{173}Tm, (which also exhibits decays to the $7/2^-$ and $9/2^-$ members of the $7/2^-[523]$ band) suggests that the 1175-keV state is a good candidate for the expected $9/2^-[514]$ intrinsic state. It should be noted that the levels proposed by Zhang *et al.* [21] to be populated in the β decay of ^{175}Er were not observed in the present work.

4. 15/2$^-$ isomer at 947 keV

A lifetime of $\tau = 64(3)$ ns was deduced for the 947-keV state from the time-difference spectrum presented in Fig. 6. Gamma-ray branches of 301 keV to the $11/2^-$ member and 164 keV to the $13/2^-$ member of the $7/2^-[523]$ band are observed, and the presence of a

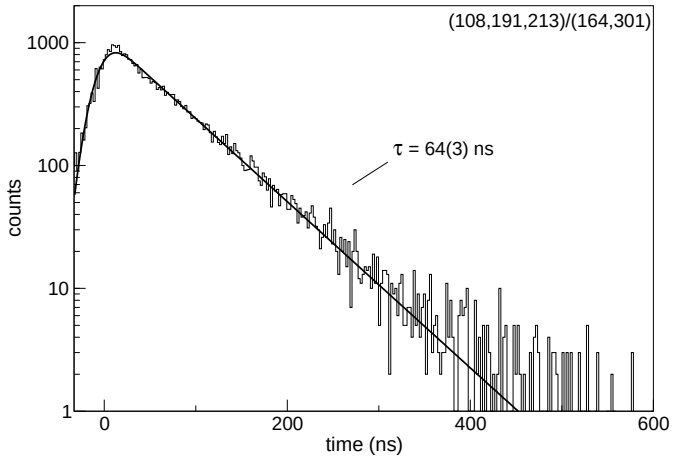

FIG. 6: Time difference spectrum measured between pairwise combinations of transitions above and below the $15/2^-$, 947-keV isomer in ^{175}Tm. A lifetime of $\tau = 64(3)$ns is deduced from a fit which includes the intrinsic time resolution.

5.2(2)-keV transition to the $15/2^-$ member is inferred from the observation of weak 159- and 295-keV γ rays in delayed coincidence with transitions above the $15/2^-$ isomer (see Fig. 1(a)). These branches limit the spin and parity to $K^\pi = 13/2^\pm$ or $15/2^\pm$.

The total conversion coefficient for the 164-keV branch was deduced from an intensity balance at the 783-keV level, using the intensities from the spectrum of Fig. 1(a). (Mixing ratios for the $E2/M1$, 137- and 159-keV γ rays are given in Table V.) The derived internal conversion coefficient of $\alpha_T(164) = 0.70(8)$ can be compared to predictions [15] of 0.09 for $E1$, 0.76 for $M1$, 0.51 for $E2$ and 4.76 for $M2$. The $E1$ and $M2$ possibilities are excluded, while an $E2$ assignment would require the 301-keV branch to be a very enhanced $M3$, which can be eliminated. This limits the 164-keV transition to be of $M1$ multipolarity while the 301-keV γ ray is most likely an $E2$ transition, resulting in a $K^\pi = 15/2^-$ assignment for the 947-keV isomer.

5. 17/2⁻ state at 1005.0 keV

A rotational band above the 947-keV, $15/2^-$ isomer was identified by a strong 191- and 213-keV cascade and a weaker, 405-keV crossover transition, low in the band (Fig. 1(b)) states are also fed by a higher-lying isomer. The band is likely to have $K^\pi = 17/2^-$, based

on the $|g_K - g_R|$ value discussed below. The 58-keV transition placed as a decay from the $17/2^-$ bandhead at 1005-keV to the 947-keV state, can be seen in the spectrum of Fig. 7(c), obtained from a 108/213-keV coincidence gate (Fig. 7(a)). The ^{174}Tm coincidence spectrum in Fig. 7(b) has been subtracted to remove the characteristic Tm X rays and, thus, isolate the 58-keV transition. By assuming that the $E2/M1$ mixing ratio for the 191-keV transition is the same as for the 213-keV transition in the same rotational band ($\delta(213\ \mathrm{keV}) = 0.31(4)$ in table V), an intensity balance for the 58- and 191-keV transitions leads to a conversion coefficient of $\alpha_T(58) = 5.3(23)$. This can be compared with predictions [15] of 0.26 for $E1$, 2.4 for $M1$ and much larger values of 26.3 for $E2$ and 80.6 for $M2$ multipolarities, respectively. All multipolarities except $M1$ can, therefore, be ruled out. Note that a small $E2/M1$ mixing ratio for the 58-keV transition would give a larger predicted conversion coefficient, closer to the experimental value. A 249-keV transition is observed in parallel with the 191- and 58-keV transitions, supporting the present placements.

The rotational band built upon the $17/2^-$ level was extended up to the $27/2^-$ member using a matrix produced with a requirement that coincidence events occurred in-beam, and also preceded 311- or 313-keV transitions by 30-800 ns.

6. $23/2^+$ isomer at 1518 keV

A lifetime of $\tau = 30(20)$ μs was measured from the spectrum of Fig. 8. The large error is a result of low statistics, due to the mismatch between the experimental chopping conditions (1 ms/3 ms) and the actual lifetime. (Note that the fit of Fig. 8 is performed beyond the distortion at the start of the spectrum.)

An intensity balance for the 108-, 213- and 405-keV transitions assuming $\delta(213\ \mathrm{keV}) = 0.31(4)$, gives $\alpha_T(108) = 0.26(4)$, to be compared with predicted values of 0.27 for $E1$, 2.47 for $M1$, 2.27 for $E2$ and 21.6 for $M2$ multipolarities, respectively. The 108-keV transition must, therefore, be of $E1$ multipolarity. The likely $M2$ assignment for the 322-keV branch results in a $K^\pi = 23/2^+$ assignment for the isomer, consistent with the reduced hindrances of the decays, as shown later in Table VII.

Due to the long lifetime, it was not possible to correlate coincidences across this isomer. Higher-lying structures in ^{175}Tm, including the expected rotational band, therefore remain unidentified, although the states above this (yrast) isomer should be populated with

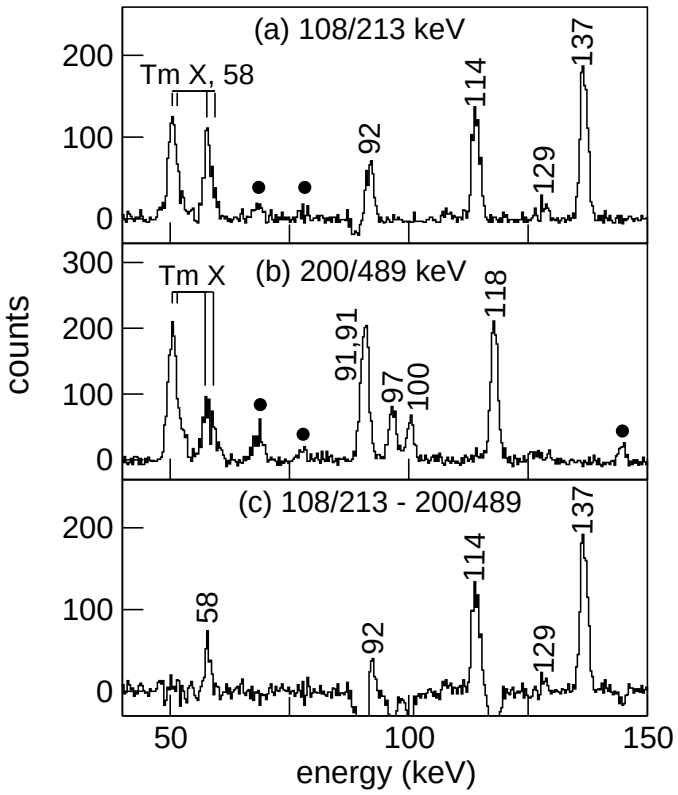

FIG. 7: Comparison of low-energy transitions in double gated γ-ray spectra for (a) ^{175}Tm and (b) ^{174}Tm. The spectra were chosen for the best possible X-ray peaks in each case. Spectrum (c) is obtained from spectrum (b) normalized and subtracted from spectrum (a), demonstrating the presence of the 58-keV transition in ^{175}Tm.

reasonably high yield.

7. Summary of energy levels and γ rays associated with ^{175}Tm

Properties of γ-ray transitions assigned to ^{175}Tm are listed in Table II, including the energies and intensities, the initial and final level energies and spin/parity assignments (where applicable). Gamma-ray intensities are normalized to the prominent 108-keV line. Since there was no single spectrum in which all out-of-beam intensities could be measured, the intensities of γ rays from each level were deduced from the measured branching ratios, taking into account the total intensity feeding into that state and γ-ray conversion coefficients from Ref. [15]. The intensity errors account for the uncertainties in branching ratios, feeding intensities and conversion coefficients.

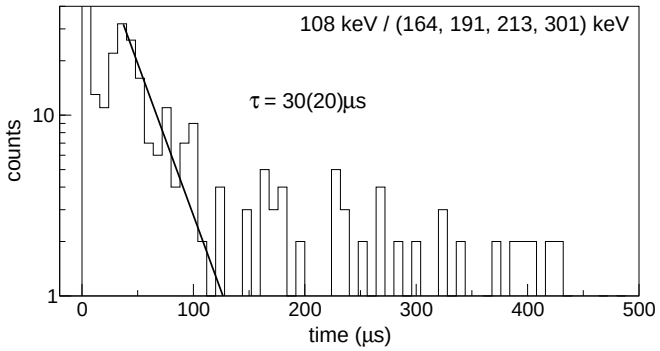

FIG. 8: Time spectrum for the sum of 108/164-keV, 108/191-keV, 108/213-keV and 108/301-keV coincidence events from the 1 ms/3 ms chopped, γ-γ-clock data with the ^{176}Yb target. Due to the very low statistics, the spectrum is compressed to $\sim$8 μs/chan.

TABLE II: Transitions assigned to ^{175}Tm.

E_γ (keV)	I_γ	E_i (keV)	E_f (keV)	K_i^π	J_i^π	K_f^π	J_f^π
5.2(2)[a]	< 0.13[b]	946.8	941.6	$\frac{15}{2}^-$	$\frac{15}{2}^-$	$\frac{7}{2}^-$	$\frac{15}{2}^-$
58.2(6)	216(81)	1005.0	946.8	$\frac{17}{2}^-$	$\frac{17}{2}^-$	$\frac{15}{2}^-$	$\frac{15}{2}^-$
87.4(4)	13(9)	440.3	353	$\frac{7}{2}^-$	$\frac{7}{2}^-$	$\frac{1}{2}^+$	$\frac{9}{2}^+$
91.9(2)	262(35)	532.2	440.3	$\frac{7}{2}^-$	$\frac{9}{2}^-$	$\frac{7}{2}^-$	$\frac{7}{2}^-$
108.3(1)	1000(56)	1517.9	1409.6	$\frac{23}{2}^+$	$\frac{23}{2}^+$	$\frac{17}{2}^-$	$\frac{21}{2}^-$
114.1(1)	379(51)	646.3	532.2	$\frac{7}{2}^-$	$\frac{11}{2}^-$	$\frac{7}{2}^-$	$\frac{9}{2}^-$
126.9(3)	221(24)[c]	127.4	0.5	$\frac{1}{2}^+$	$\frac{5}{2}^+$	$\frac{1}{2}^+$	$\frac{3}{2}^+$
127(1)	[c]	127.4	0	$\frac{1}{2}^+$	$\frac{5}{2}^+$	$\frac{1}{2}^+$	$\frac{1}{2}^+$
128.8(2)	302(33)	129.3	0.5	$\frac{1}{2}^+$	$\frac{7}{2}^+$	$\frac{1}{2}^+$	$\frac{3}{2}^+$
136.8(1)	419(48)	783.0	646.3	$\frac{7}{2}^-$	$\frac{13}{2}^-$	$\frac{7}{2}^-$	$\frac{11}{2}^-$
158.6(2)	38(6)	941.6	783.0	$\frac{7}{2}^-$	$\frac{15}{2}^-$	$\frac{7}{2}^-$	$\frac{13}{2}^-$

[a] Transition unobserved, inferred from coincidence observations.

[b] Intensity inferred from intensity balances.

[c] Transition intensities of doublet transitions cannot be resolved.

TABLE II – continued

E_γ (keV)	I_γ	E_i (keV)	E_f (keV)	K_i^π	J_i^π	K_f^π	J_f^π
163.8(1)	566(35)	946.8	783.0	$\frac{15}{2}^-$	$\frac{15}{2}^-$	$\frac{7}{2}^-$	$\frac{13}{2}^-$
181.6(3)		1123.3	941.6	$\frac{7}{2}^-$	$\frac{17}{2}^-$	$\frac{7}{2}^-$	$\frac{15}{2}^-$
191.2(1)	822(71)	1196.2	1005.0	$\frac{17}{2}^-$	$\frac{19}{2}^-$	$\frac{17}{2}^-$	$\frac{17}{2}^-$
200.5(5)		1324.1	1123.3	$\frac{7}{2}^-$	$\frac{19}{2}^-$	$\frac{7}{2}^-$	$\frac{17}{2}^-$
206.2(2)	42(8)	646.3	440.3	$\frac{7}{2}^-$	$\frac{11}{2}^-$	$\frac{7}{2}^-$	$\frac{7}{2}^-$
213.4(1)	843(71)	1409.6	1196.2	$\frac{17}{2}^-$	$\frac{21}{2}^-$	$\frac{17}{2}^-$	$\frac{19}{2}^-$
224(1)	7(5)	353	129.3	$\frac{1}{2}^+$	$\frac{9}{2}^+$	$\frac{1}{2}^+$	$\frac{7}{2}^+$
226(1)	7(5)	353	127.4	$\frac{1}{2}^+$	$\frac{9}{2}^+$	$\frac{1}{2}^+$	$\frac{5}{2}^+$
229.5(2)		358.8	129.3	$\frac{1}{2}^+$	$\frac{11}{2}^+$	$\frac{1}{2}^+$	$\frac{7}{2}^+$
235.1(3)		1644.7	1409.6	$\frac{17}{2}^-$	$\frac{23}{2}^-$	$\frac{17}{2}^-$	$\frac{21}{2}^-$
249(1)	9(5)	1196.2	946.8	$\frac{17}{2}^-$	$\frac{19}{2}^-$	$\frac{15}{2}^-$	$\frac{15}{2}^-$
250.9(2)	105(15)	783.0	532.2	$\frac{7}{2}^-$	$\frac{13}{2}^-$	$\frac{7}{2}^-$	$\frac{9}{2}^-$
255.5(4)		1900.2	1644.7	$\frac{17}{2}^-$	$\frac{25}{2}^-$	$\frac{17}{2}^-$	$\frac{23}{2}^-$
259(1)		1433.6	1175			$(\frac{9}{2}^-)$	$(\frac{9}{2}^-)$
276(1)		2176	1900.2	$\frac{17}{2}^-$	$\frac{27}{2}^-$	$\frac{17}{2}^-$	$\frac{25}{2}^-$
295.4(2)	18(4)	941.6	646.3	$\frac{7}{2}^-$	$\frac{15}{2}^-$	$\frac{7}{2}^-$	$\frac{11}{2}^-$
300.6(1)	255(18)	946.8	646.3	$\frac{15}{2}^-$	$\frac{15}{2}^-$	$\frac{7}{2}^-$	$\frac{11}{2}^-$
311.0(2)	743(82)	440.3	129.3	$\frac{7}{2}^-$	$\frac{7}{2}^-$	$\frac{1}{2}^+$	$\frac{7}{2}^+$
313.0(2)	553(61)	440.3	127.4	$\frac{7}{2}^-$	$\frac{7}{2}^-$	$\frac{1}{2}^+$	$\frac{5}{2}^+$
316(1)		675	358.8	$\frac{1}{2}^+$	$\frac{13}{2}^+$	$\frac{1}{2}^+$	$\frac{11}{2}^+$
321.7(2)	53(10)	1517.9	1196.2	$\frac{23}{2}^+$	$\frac{23}{2}^+$	$\frac{17}{2}^-$	$\frac{19}{2}^-$
322(1)		675	353	$\frac{1}{2}^+$	$\frac{13}{2}^+$	$\frac{1}{2}^+$	$\frac{9}{2}^+$
326.7(3)		685.5	358.8	$\frac{1}{2}^+$	$\frac{15}{2}^+$	$\frac{1}{2}^+$	$\frac{11}{2}^+$

[a] Transition unobserved, inferred from coincidence observations.

[b] Intensity inferred from intensity balances.

[c] Transition intensities of doublet transitions cannot be resolved.

TABLE II – continued

E_γ (keV)	I_γ	E_i (keV)	E_f (keV)	K_i^π	J_i^π	K_f^π	J_f^π
340.2(3)		1123.3	783.0	$\frac{7}{2}^-$	$\frac{17}{2}^-$	$\frac{7}{2}^-$	$\frac{13}{2}^-$
382.2(4)		1324.1	941.6	$\frac{7}{2}^-$	$\frac{19}{2}^-$	$\frac{7}{2}^-$	$\frac{15}{2}^-$
398(1)		1084	685.5	$\frac{1}{2}^+$	$\frac{17}{2}^+$	$\frac{1}{2}^+$	$\frac{15}{2}^+$
404.6(2)	126(16)	1409.6	1005.0	$\frac{17}{2}^-$	$\frac{21}{2}^-$	$\frac{17}{2}^-$	$\frac{17}{2}^-$
409(1)		1084	675	$\frac{1}{2}^+$	$\frac{17}{2}^+$	$\frac{1}{2}^+$	$\frac{13}{2}^+$
418.4(4)		1103.9	685.5	$\frac{1}{2}^+$	$\frac{19}{2}^+$	$\frac{1}{2}^+$	$\frac{15}{2}^+$
440(1)	13(8)	440.3	0.5	$\frac{7}{2}^-$	$\frac{7}{2}^-$	$\frac{1}{2}^+$	$\frac{3}{2}^+$
448.5(3)		1644.7	1196.2	$\frac{17}{2}^-$	$\frac{23}{2}^-$	$\frac{17}{2}^-$	$\frac{19}{2}^-$
490.6(4)		1900.2	1409.6	$\frac{17}{2}^-$	$\frac{25}{2}^-$	$\frac{17}{2}^-$	$\frac{21}{2}^-$
502.4(4)		1606.3	1103.9	$\frac{1}{2}^+$	$\frac{23}{2}^+$	$\frac{1}{2}^+$	$\frac{19}{2}^+$
513(1)	12(7)	1517.9	1005.0	$\frac{23}{2}^+$	$\frac{23}{2}^+$	$\frac{17}{2}^-$	$\frac{17}{2}^-$
532(1)		2176	1644.7	$\frac{17}{2}^-$	$\frac{27}{2}^-$	$\frac{17}{2}^-$	$\frac{23}{2}^-$
643(1)		1175	532.2	$(\frac{9}{2}^-)$	$(\frac{9}{2}^-)$	$\frac{7}{2}^-$	$\frac{9}{2}^-$
690.6(3)		2124.2	1433.6				
735(1)		1175	440.3	$(\frac{9}{2}^-)$	$(\frac{9}{2}^-)$	$\frac{7}{2}^-$	$\frac{7}{2}^-$
993.3(3)		1433.6	440.3			$\frac{7}{2}^-$	$\frac{7}{2}^-$

[a] Transition unobserved, inferred from coincidence observations.

[b] Intensity inferred from intensity balances.

[c] Transition intensities of doublet transitions cannot be resolved.

B. ^{173}Tm

Figure 9 presents γ-ray spectra associated with ^{173}Tm that are observed out of beam with the ^{176}Yb target. The proposed ^{173}Tm level scheme is found in Fig. 10.

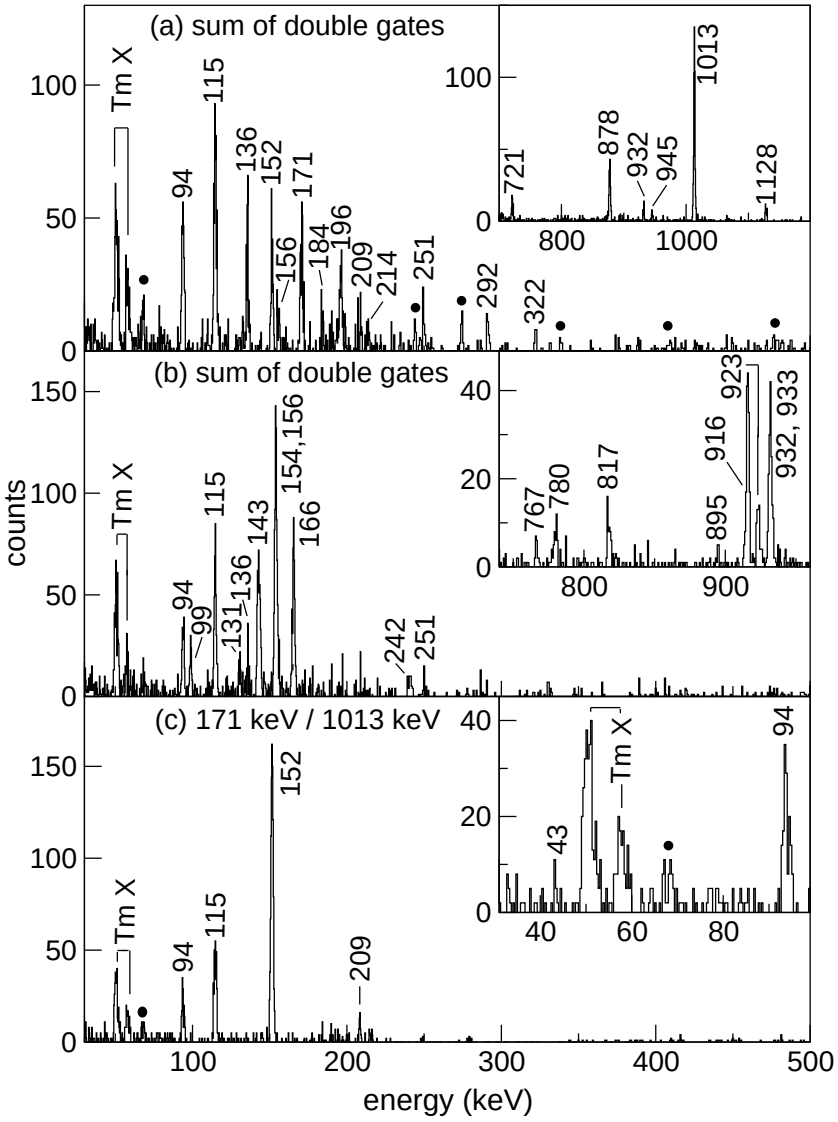

FIG. 9: Coincidence spectra showing transitions in ^{173}Tm. (a): The spectrum resulting from a sum of 152/171-keV and 115/1013-keV double coincidence gates. Inset: 700-1200-keV energy region (b): Spectrum obtained from a sum of double gates on 166-keV/(154,916,923,932)-keV and 143-keV/(154,916,932)-keV γ-ray pairs. Inset: 750-950-keV energy region. (c): A 171/1013-keV gated spectrum used for the intensity balance on the 43-keV transition. The weak 43-keV transition is shown in the expanded inset. Contaminants are labelled by filled circles.

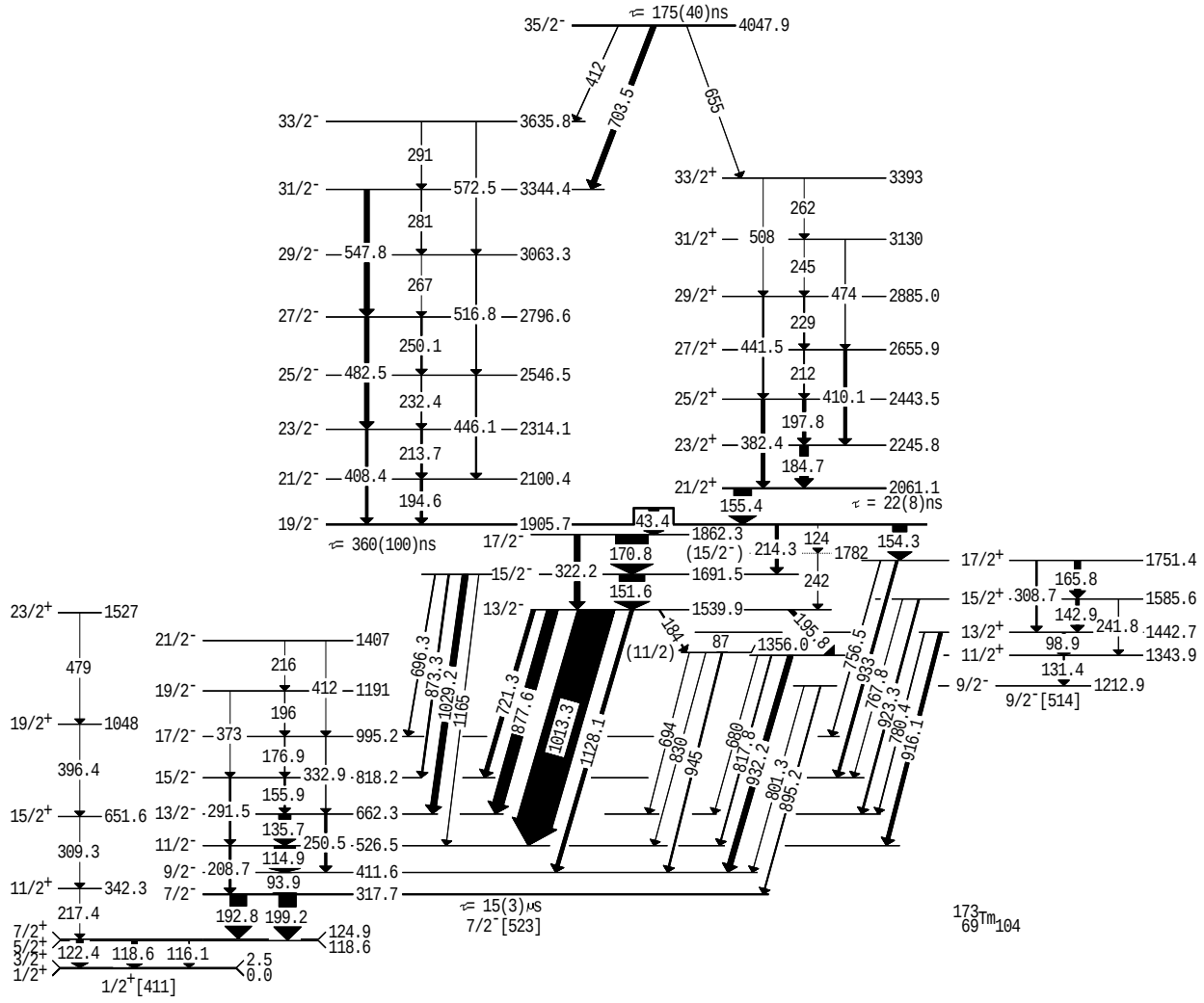

FIG. 10: The proposed level scheme for ^{173}Tm. Arrow widths represent the relative γ-ray intensities. The intensities for the $21/2^+$ band include in-beam relative intensities, in order to highlight the in-band branching ratios.

1. *1/2⁺[411], ground state band*

The present results are consistent with the ground-state band assignments of Pursiheimo *et al.* [23] up to the $7/2^+$ state. An energy of 342.3(3) keV for the $11/2^+$ state is consistent with the value of 339.8(25) keV for the $9/2^+$, $11/2^+$ doublet from Tarara *et al.* [24]. The $3/2^+$, $7/2^+$, $11/2^+$... sequence of levels (α=$-1/2$ signature) has been extended up to the $23/2^+$ member. The $1/2^+$, $5/2^+$, $9/2^+$... sequence (α=$+1/2$ signature) had insufficient intensity for an extension above the $5/2^+$ state, which was strongly fed by the $7/2^-$ isomer.

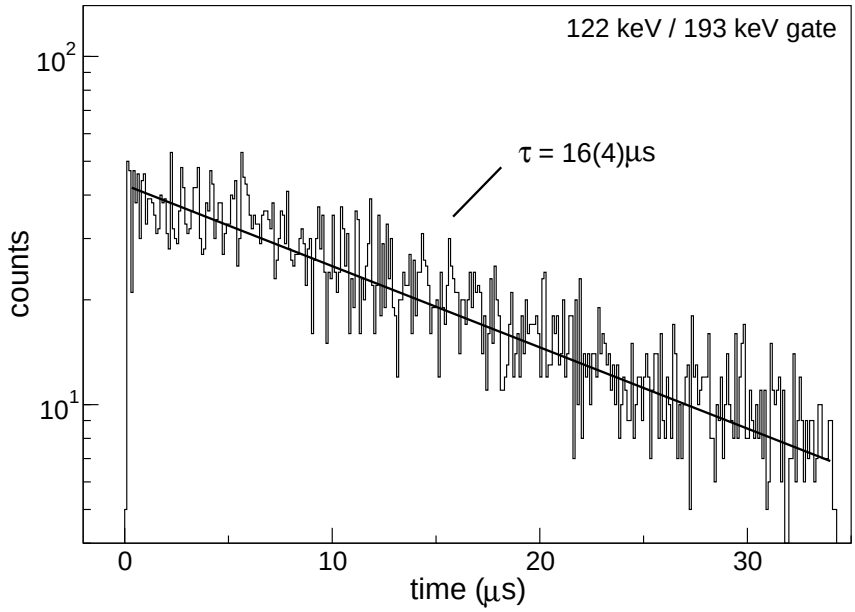

FIG. 11: A time spectrum showing 122/193-keV γ-ray coincidences relative to the chopped beam from the ^{176}Lu, 10μs/40μs, γ-γ-clock data. The spectrum shows the decay curve for the $7/2^-$ isomer in ^{173}Tm.

The γ rays tentatively assigned to the α=$-1/2$ signature band by Asztalos *et al.* [25] have not been observed in the present data.

2. 7/2⁻[523] isomer at 318 keV

Figure 11 provides a decay curve for the $7/2^-[523]$ isomer. The fit results in a lifetime of $\tau = 16(4)$ μs, consistent with the value of $\tau = 14(3)$ μs measured by Pursiheimo *et al.* [23]. A weighted mean of $\tau = 15(3)$ μs is adopted for the lifetime of this level.

The current $7/2^-$ and $9/2^-$ level assignments in the $7/2^-[523]$ rotational band agree with those of Ref. [23]. The present data also agree, within error, with the extensions of Tarara *et al.* [24] up to the $11/2^-$ state, but their energy of 669.5(17) keV for the $13/2^-$ level does not agree with the present value of 662.3(2) keV. The present assignments extend the rotational band up to the $17/2^-$ member in the out-of-beam data, and to the $21/2^-$ member using in-beam information.

3. *9/2⁻[514] state at 1213 keV*

The present work confirms the observation of this state by Pursiheimo *et al.* [23]. It is fed weakly from the 1344-keV level, and decays via 801- and 895-keV branches to the $7/2^-$ and $9/2^-$ members of the $7/2^-[523]$ band.

4. *Positive parity states at 1344, 1443, 1586 and 1751 keV*

The 1344-keV level decays via high-energy transitions to the $7/2^-[523]$ band and via a 131-keV transition to the $9/2^-[514]$ state. The 131-keV transition was observed only weakly, therefore, several independent intensity balances were performed, resulting in a conversion coefficient limit of $\alpha_T(131) \leq 0.44$ to be compared with predictions [15] of 0.16 for $E1$, 1.42 for $M1$, 1.12 for $E2$ and 10.57 for $M2$ multipolarities, respectively. This leads to an unambiguous $E1$ assignment for the 131-keV transition and a positive parity for the 1344-keV level.

The energy difference of 99 keV between the 1344- and 1443-keV levels seems too small for the 1443-keV level to be a band member. However, the states at 1586- and 1751-keV have the appearance of a rotational band built on the 1443-keV state. If this is in fact not a band, it should be considered whether either of the 241.8- or 308.7-keV transitions is of $M2$ character. The limits on the implied lifetime (taking an $M2$ transition strength limit of ≤ 1 W.u.) would then be $\tau \geq 57$ ns for the 1751-keV state, and $\tau \geq$76 ns for the 1586-keV level. However, limits of $\tau < 5$ ns are established for the 1344-, 1443-, 1586- and 1751-keV level lifetimes from time-difference data. The 242- and 309-keV transitions must, therefore, be of $E2$ character, requiring all four levels to be of positive parity.

Each of these positive parity states is connected to the $7/2^-[523]$ band by high energy E1 transitions. (M2 multipolarities can be ruled out on inspection of the inter-band transition branching ratios.) The E1 assignments limit the spin and parity to $11/2^+$ for the 1344 keV level and $13/2^+$ for the 1443 keV level. The inter-band decays from the $15/2^+$ (1586 keV) and $17/2^+$ (1751 keV) members of the $13/2^+$ rotational band are K-forbidden E1 transitions. Their competition with in-band collective transitions will be discussed below.

5. 13/2⁻ state at 1540 keV

Several branches are observed from this level, the most intense being the high-energy, inter-band transitions to the $7/2^-[523]$ band. The branching ratios of these transitions restrict the spin and parity to $J^\pi = 13/2^\pm$. The state appears to have an associated rotational band with levels at 1692 and 1862 keV, that are fed by 214- and 43-keV transitions from the 1906-keV, $19/2^-$ isomer, respectively (see below for the spin/parity assignment for the $19/2^-$ isomer). The spin/parity assignments for the 1540-, 1692- and 1862-keV levels can be constrained further from the multipolarity of the 43- or 214-keV transitions. Assuming that the $E2/M1$ mixing ratio for the 152-keV transition is consistent with that of the 171-keV transition in the same rotational band ($\delta(171\text{ keV}) = 0.29(3)$ in table IV), an intensity balance for the 43- and 152-keV γ rays in the 171/1013-keV double gated spectrum of Fig. 9(c) results in $\alpha_T(43) = 8.8^{+10.3}_{-3.6}$, with the large uncertainty following from the low statistics in the 43-keV peak and the uncertainty in the efficiency calibration below 60 keV. Comparison to predictions [15] of 0.59 for $E1$, 5.77 for $M1$, 109.9 for $E2$ and 296 for $M2$ multipolarities, respectively, suggests that only an $M1$ multipolarity is consistent (albeit within a large uncertainty), requiring negative parity for the 1540-, 1692- and 1862-keV levels.

6. (15/2⁻) state at (1782 keV)

The excitation energy of this level (at 1664 or 1782 keV) is ambiguous, due to the inability to order the 124- and 242-keV transitions. Given the observation of a single branch to a $J^\pi = 13/2^-$ state, it is very likely to be an intrinsic state of negative parity. The most probable assignments are $K = 15/2$ or $17/2$. An assignment of $K^\pi = (15/2^-)$, and an excitation energy of 1782 keV are tentatively favored from hindrance arguments for the 1906-keV isomer decays.

7. 19/2⁻ isomer at 1906 keV

The lifetime of this state is deduced to be $\tau = 360(100)$ ns from the time-difference spectrum in Fig. 12. The lifetime fit starts at 50 ns, in order to avoid a possible prompt

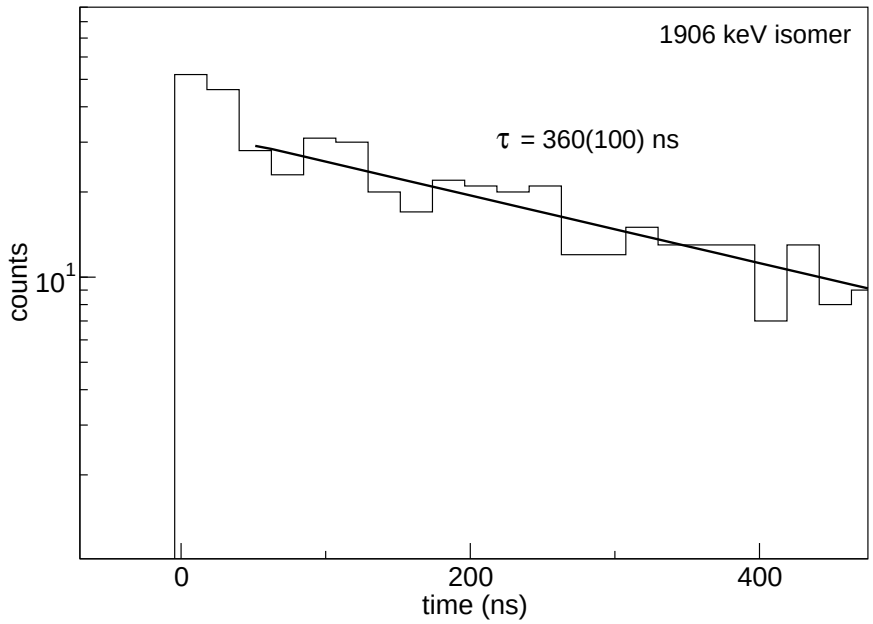

FIG. 12: A sum of time-difference spectra between the 1013-keV γ ray, and the 408, 548 and 704-keV transitions in ^{173}Tm. Due to the very low statistics, the time spectrum was compressed to 20 ns/chan.

contaminant component at the start of the time curve.

The isomer is characterized by several decay branches, the strongest (in total intensity) being the 43-keV, $M1$ transition to the 1862-keV state, and the 154-keV transition to the 1751-keV, $17/2^+$ level. In order to find the spin/parity assignment for the isomer at 1906 keV, two independent intensity balances were performed for the 154-keV decay branch using $E2/M1$ mixing ratios deduced from Table IV. In the first, the 154-keV transition was balanced against the sum of 115- and 209-keV transition intensities in a sum of (143,166,309)/916-keV double gated spectra, leading to $\alpha_T(154) = 0.07(31)$. In the second, the 154- and 166-keV transitions were balanced in a spectrum produced from a sum of 143/(780,818,916,932)-keV double gates, leading to $\alpha_T(154) = 0.04(27)$. Predicted values of 0.11 ($E1$), 0.90 ($M1$), 0.63 ($E2$) and 5.9 ($M2$) confirm an $E1$ assignment. A strong $E1$ branch to the 1586-keV level would also be expected if the isomer had an assignment of $17/2^-$ or lower, therefore the spin and parity is restricted to $K^\pi = 19/2^-$.

Structures above the isomer were studied by examining γ rays both in- and out-of-beam that were measured 30-800 ns early with respect to the intense 1013-keV transition. The rotational band built on the 1906-keV, $19/2^-$ state was identified in this way. It is fed by a

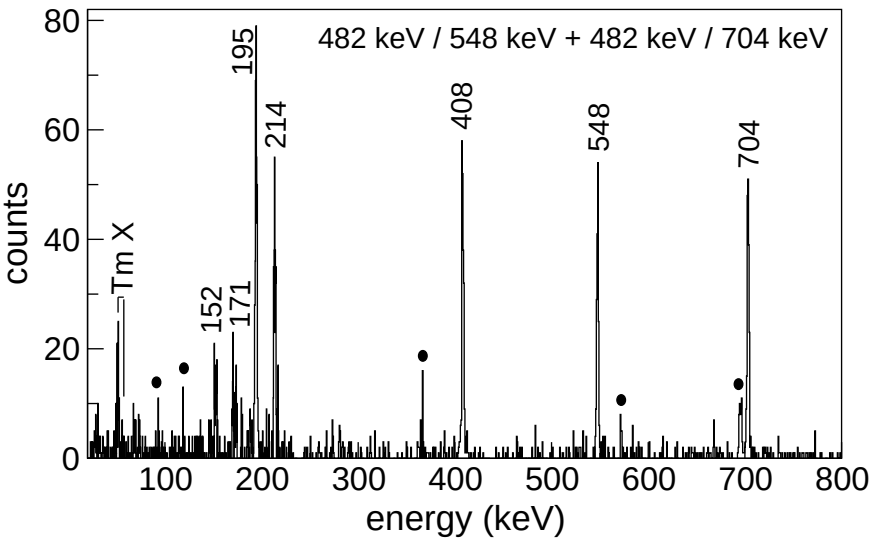

FIG. 13: Spectrum showing the rotational band built on the $19/2^-$, 1906-keV state in ^{173}Tm, obtained from a sum of 482/548- and 482/704-keV double gates in the out-of-beam γ-γ-γ cube. Contaminants are labelled with filled circles.

higher-lying isomer, and is clear in a sum of double gated spectra in the out-of-beam, γ-γ-γ cube in Fig. 13. The spectrum also shows the 152- and 171-keV lines from below the isomer in weak coincidence (across the 360(100) ns isomer).

8. $21/2^+$ isomer at 2061 keV

The transitions associated with the band built on the 2061-keV state are presented in Figs. 14(a) and (b). The 2061-keV level has a single, 155-keV decay branch to the $19/2^-$ isomer at 1906 keV. By assuming that the $E2/M1$ mixing ratio for the 185-keV transition is the same as for the 198-keV transition in the same rotational band (δ(198 keV) = 1.41(40) in table IV), an intensity balance was performed for the 155-, 185- and 382-keV transitions using spectrum 14(a), yielding $\alpha_T(155) = 0.08(17)$. Predicted values of 0.10 ($E1$), 0.89 ($M1$), 0.62 ($E2$) and 5.8 ($M2$) suggest an $E1$ assignment, making the 2061-keV level either $J^\pi = 19/2^+$ or $21/2^+$. A $K^\pi = 21/2^+$ assignment is strongly favored from the $|g_K - g_R|$ value, and the three-quasiparticle states expected in this nucleus (see further discussion below).

In order to measure the lifetime of the $21/2^+$ state, a γ-beam matrix was constructed requiring γ rays that are observed 30 to 800 ns early with respect to 152/1013-keV or

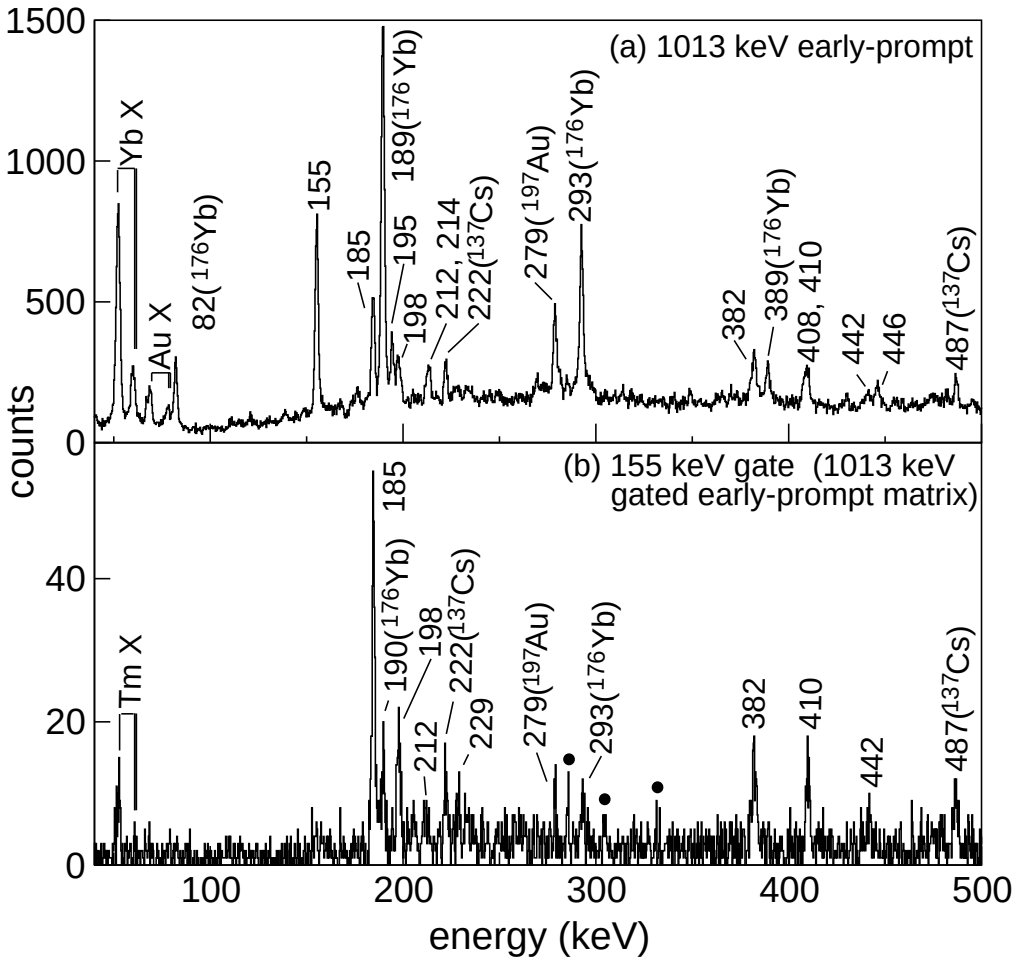

FIG. 14: Spectra showing γ rays from the $21/2^+$ band in ^{173}Tm. (a) Spectrum sorted with a requirement that events occur in-beam, and 30-800 ns early with respect to an out-of-beam 1013-keV transition. (b) A 155-keV gated spectrum from a matrix produced by projecting in-beam coincidence pairs that are detected 30-800 ns earlier than an out-of-beam 1013-keV transition. Contaminants are labelled with filled circles.

171/1013-keV γ-ray pairs. A gate on the 155-keV line in this matrix gives the absolute time spectrum for this γ ray with respect to the beam pulse, and is found in Fig. 15. A lifetime of 22(8) ns was deduced for the 2061-keV state.

9. 35/2$^-$ isomer at 4048 keV

The 4048-keV isomer decays by a strong 704-keV transition to the $31/2^-$ member of the $19/2^-$ band, and a much weaker 412-keV branch to the $33/2^-$ member, as well as a weak,

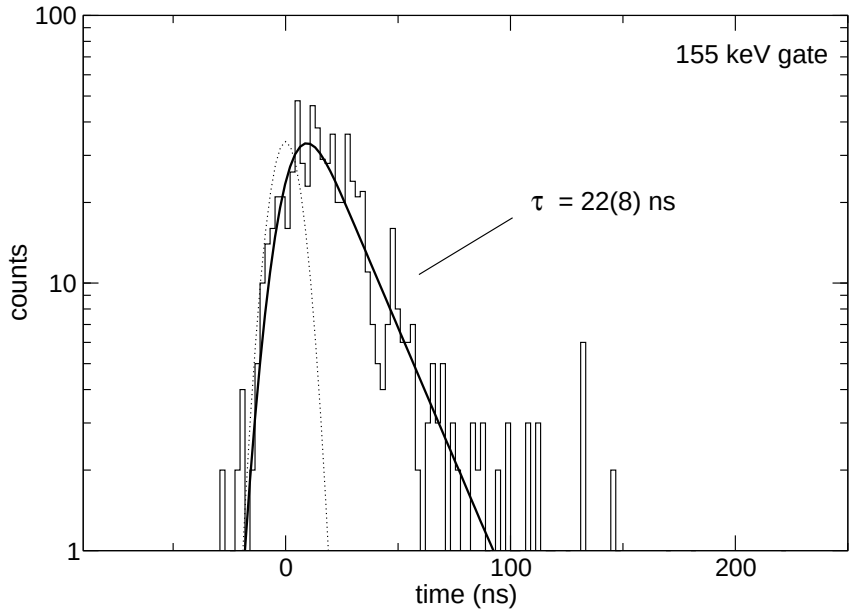

FIG. 15: Time curve for the $21/2^+$ isomer in ^{173}Tm, produced from a 155-keV gate in a γ-beam matrix. The dotted line represents the time curve for a prompt γ ray with a similar energy.

655-keV branch to the $33/2^+$ member of the $21/2^+$ band. These branches, along with the non-observation of a decay to the $31/2^+$ level at 3130 keV, imply a likely spin and parity of $35/2^{\pm}$. The $35/2^+$ option would imply that the 704-keV transition is of $M2$ character,

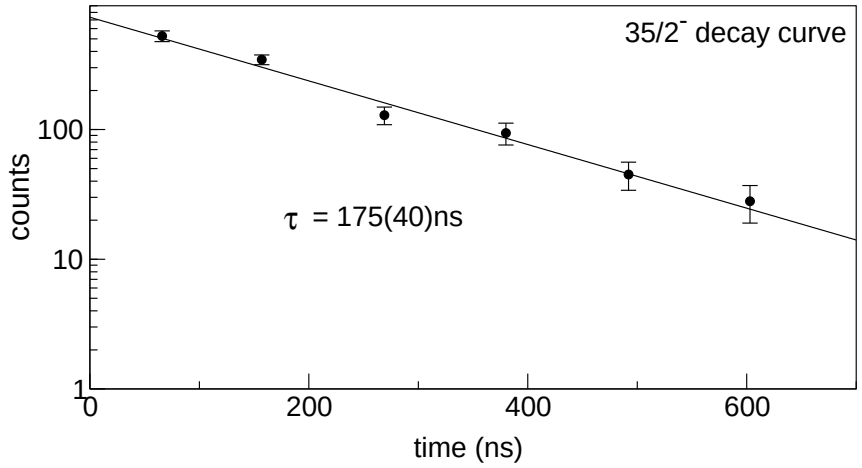

FIG. 16: A time curve for the $35/2^-$ isomer in ^{173}Tm. The points represent the sum of 195-, 214-, 408- and 483-keV γ-ray intensities from 548/704-keV double gated spectra, from six contiguous time regions in the out-of-beam data.

with a strength that is only consistent with a transition between specific one-quasiparticle configurations and, therefore, very unlikely in the present case. A $K^\pi = 35/2^-$ assignment is, therefore, adopted for this state. A lifetime of $\tau = 175(40)$ ns was determined for the $35/2^-$ isomer from the fit in Fig. 16.

10. Summary of energy levels and γ rays associated with ^{173}Tm

Properties including γ-ray energies and intensities, initial and final level energies and spin/parity assignments of transitions assigned to ^{173}Tm are summarized in Table III. Gamma-ray intensities are normalized to the prominent 171-keV line. As for ^{175}Tm (Table II), the intensities of γ rays from each level were deduced from the measured branching ratios, taking into account the total intensity feeding into that state and γ-ray conversion coefficients from Ref. [15]. The quoted intensity errors account for the uncertainties in branching ratios, feeding intensities and conversion coefficients.

TABLE III: Transitions assigned to ^{173}Tm.

E_γ (keV)	I_γ	E_i (keV)	E_f (keV)	K_i^π	J_i^π	K_f^π	J_f^π
43.4(6)	272(68)[a]	1905.7	1862.3	$\frac{19}{2}^-$	$\frac{19}{2}^-$	$\frac{13}{2}^-$	$\frac{17}{2}^-$
87(1)	5(3)	1442.7	1356	$\frac{13}{2}^+$	$\frac{13}{2}^+$	$(\frac{11}{2})$	$(\frac{11}{2})$
93.9(1)	526(104)	411.6	317.7	$\frac{7}{2}^-$	$\frac{9}{2}^-$	$\frac{7}{2}^-$	$\frac{7}{2}^-$
98.9(3)	33(10)	1442.7	1343.9	$\frac{13}{2}^+$	$\frac{13}{2}^+$	$\frac{11}{2}^+$	$\frac{11}{2}^+$
114.9(1)	695(132)	526.5	411.6	$\frac{7}{2}^-$	$\frac{11}{2}^-$	$\frac{7}{2}^-$	$\frac{9}{2}^-$
116.1(3)	23(8)	118.6	2.5	$\frac{1}{2}^+$	$\frac{5}{2}^+$	$\frac{1}{2}^+$	$\frac{3}{2}^+$
118.6(2)	181(30)	118.6	0	$\frac{1}{2}^+$	$\frac{5}{2}^+$	$\frac{1}{2}^+$	$\frac{1}{2}^+$
122.4(2)	211(35)	124.9	2.5	$\frac{1}{2}^+$	$\frac{7}{2}^+$	$\frac{1}{2}^+$	$\frac{3}{2}^+$
124(1)	9(5)	1905.7	(1782)	$\frac{19}{2}^-$	$\frac{19}{2}^-$	$(\frac{15}{2}^-)$	$(\frac{15}{2}^-)$
131.4(3)	41(14)	1343.9	1212.9	$\frac{11}{2}^+$	$\frac{11}{2}^+$	$\frac{9}{2}^-$	$\frac{9}{2}^-$
135.7(1)	373(80)	662.3	526.5	$\frac{7}{2}^-$	$\frac{13}{2}^-$	$\frac{7}{2}^-$	$\frac{11}{2}^-$

[a] Intensity inferred from intensity balances .

TABLE III – continued

E_γ (keV)	I_γ	E_i (keV)	E_f (keV)	K_i^π	J_i^π	K_f^π	J_f^π
142.9(2)	112(20)	1585.6	1442.7	$\frac{13}{2}^+$	$\frac{15}{2}^+$	$\frac{13}{2}^+$	$\frac{13}{2}^+$
151.6(1)	780(84)	1691.5	1539.9	$\frac{13}{2}^-$	$\frac{15}{2}^-$	$\frac{13}{2}^-$	$\frac{13}{2}^-$
154.3(2)	440(44)	1905.7	1751.4	$\frac{19}{2}^-$	$\frac{19}{2}^-$	$\frac{13}{2}^-$	$\frac{17}{2}^-$
155.4(1)		2061.1	1905.7	$\frac{21}{2}^+$	$\frac{21}{2}^+$	$\frac{19}{2}^-$	$\frac{19}{2}^-$
155.9(1)	143(39)	818.2	662.3	$\frac{7}{2}^-$	$\frac{15}{2}^-$	$\frac{7}{2}^-$	$\frac{13}{2}^-$
165.8(3)	189(27)	1751.4	1585.6	$\frac{13}{2}^+$	$\frac{17}{2}^+$	$\frac{13}{2}^+$	$\frac{15}{2}^+$
170.8(1)	1000(58)	1862.3	1691.5	$\frac{13}{2}^-$	$\frac{17}{2}^-$	$\frac{13}{2}^-$	$\frac{15}{2}^-$
176.9(3)	26(13)	995.2	818.2	$\frac{7}{2}^-$	$\frac{17}{2}^-$	$\frac{7}{2}^-$	$\frac{15}{2}^-$
184(1)	45(11)	1539.9	1356	$\frac{13}{2}^-$	$\frac{13}{2}^-$	$(\frac{11}{2})$	$(\frac{11}{2})$
184.7(1)		2245.8	2061.1	$\frac{23}{2}^+$	$\frac{21}{2}^+$	$\frac{21}{2}^+$	$\frac{21}{2}^+$
192.8(2)	516(50)	317.7	124.9	$\frac{7}{2}^-$	$\frac{7}{2}^-$	$\frac{1}{2}^+$	$\frac{7}{2}^+$
194.6(1)	298(104)	2100.4	1905.7	$\frac{19}{2}^-$	$\frac{21}{2}^-$	$\frac{19}{2}^-$	$\frac{19}{2}^-$
195.8(2)	132(27)	1539.9	1343.9	$\frac{13}{2}^-$	$\frac{13}{2}^-$	$\frac{11}{2}^+$	$\frac{11}{2}^+$
196(1)		1191	995.2	$\frac{7}{2}^-$	$\frac{19}{2}^-$	$\frac{7}{2}^-$	$\frac{17}{2}^-$
197.8(2)		2443.5	2245.8	$\frac{21}{2}^+$	$\frac{25}{2}^+$	$\frac{21}{2}^+$	$\frac{23}{2}^+$
199.2(2)	532(50)	317.7	118.6	$\frac{7}{2}^-$	$\frac{7}{2}^-$	$\frac{1}{2}^+$	$\frac{5}{2}^+$
208.7(2)	63(15)	526.5	317.7	$\frac{7}{2}^-$	$\frac{11}{2}^-$	$\frac{7}{2}^-$	$\frac{7}{2}^-$
212(1)		2655.9	2443.5	$\frac{21}{2}^+$	$\frac{27}{2}^+$	$\frac{21}{2}^+$	$\frac{25}{2}^+$
213.7(1)	196(60)	2314.1	2100.4	$\frac{19}{2}^-$	$\frac{23}{2}^-$	$\frac{19}{2}^-$	$\frac{21}{2}^-$
214.3(4)	102(15)	1905.7	1691.5	$\frac{19}{2}^-$	$\frac{19}{2}^-$	$\frac{13}{2}^-$	$\frac{15}{2}^-$
216(1)		1407	1191	$\frac{7}{2}^-$	$\frac{21}{2}^-$	$\frac{7}{2}^-$	$\frac{19}{2}^-$
217.4(3)		342.3	124.9	$\frac{1}{2}^+$	$\frac{11}{2}^+$	$\frac{1}{2}^+$	$\frac{7}{2}^+$
229(1)		2885	2655.9	$\frac{21}{2}^+$	$\frac{29}{2}^+$	$\frac{21}{2}^+$	$\frac{27}{2}^+$
232.4(4)	46(27)	2546.5	2314.1	$\frac{19}{2}^-$	$\frac{25}{2}^-$	$\frac{19}{2}^-$	$\frac{23}{2}^-$
241.8(6)	14(4)	1585.6	1343.9	$\frac{13}{2}^+$	$\frac{15}{2}^+$	$\frac{11}{2}^+$	$\frac{11}{2}^+$

[a] Intensity inferred from intensity balances .

TABLE III – continued

E_γ (keV)	I_γ	E_i (keV)	E_f (keV)	K_i^π	J_i^π	K_f^π	J_f^π
242(1)	15(8)	(1782)	1539.9	$(\frac{15}{2}^-)$	$(\frac{15}{2}^-)$	$\frac{13}{2}^-$	$\frac{13}{2}^-$
245(1)		3130	2885	$\frac{21}{2}^+$	$\frac{31}{2}^+$	$\frac{21}{2}^+$	$\frac{29}{2}^+$
250.1(4)	87(25)	2796.6	2546.5	$\frac{19}{2}^-$	$\frac{27}{2}^-$	$\frac{19}{2}^-$	$\frac{25}{2}^-$
250.5(2)	71(7)	662.3	411.6	$\frac{7}{2}^-$	$\frac{13}{2}^-$	$\frac{7}{2}^-$	$\frac{9}{2}^-$
262(1)		3393	3130	$\frac{21}{2}^+$	$\frac{33}{2}^+$	$\frac{21}{2}^+$	$\frac{31}{2}^+$
267(1)	15(12)	3063.3	2796.6	$\frac{19}{2}^-$	$\frac{29}{2}^-$	$\frac{19}{2}^-$	$\frac{27}{2}^-$
281(1)	57(18)	3344.4	3063.3	$\frac{19}{2}^-$	$\frac{31}{2}^-$	$\frac{19}{2}^-$	$\frac{29}{2}^-$
291(1)	4(3)	3635.8	3344.4	$\frac{19}{2}^-$	$\frac{33}{2}^-$	$\frac{19}{2}^-$	$\frac{31}{2}^-$
291.5(1)	51(15)	818.2	662.3	$\frac{7}{2}^-$	$\frac{15}{2}^-$	$\frac{7}{2}^-$	$\frac{11}{2}^-$
308.7(4)	54(11)	1751.4	1442.7	$\frac{13}{2}^+$	$\frac{17}{2}^+$	$\frac{13}{2}^+$	$\frac{13}{2}^+$
309.3(3)		651.6	342.3	$\frac{1}{2}^+$	$\frac{15}{2}^+$	$\frac{1}{2}^+$	$\frac{11}{2}^+$
322.2(3)	180(14)	1862.3	1539.9	$\frac{13}{2}^-$	$\frac{17}{2}^-$	$\frac{13}{2}^-$	$\frac{13}{2}^-$
332.9(4)	16(8)	995.2	662.3	$\frac{7}{2}^-$	$\frac{17}{2}^-$	$\frac{7}{2}^-$	$\frac{13}{2}^-$
373(1)		1191	818.2	$\frac{7}{2}^-$	$\frac{19}{2}^-$	$\frac{7}{2}^-$	$\frac{15}{2}^-$
382.4(2)		2443.5	2061.1	$\frac{21}{2}^+$	$\frac{25}{2}^+$	$\frac{21}{2}^+$	$\frac{21}{2}^+$
396.4(4)		1048.0	651.6	$\frac{1}{2}^+$	$\frac{19}{2}^+$	$\frac{1}{2}^+$	$\frac{15}{2}^+$
408.4(1)	257(77)	2314.1	1905.7	$\frac{19}{2}^-$	$\frac{23}{2}^-$	$\frac{19}{2}^-$	$\frac{19}{2}^-$
410.1(2)		2655.9	2245.8	$\frac{21}{2}^+$	$\frac{27}{2}^+$	$\frac{21}{2}^+$	$\frac{23}{2}^+$
412(1)		1407	995.2	$\frac{7}{2}^-$	$\frac{21}{2}^-$	$\frac{7}{2}^-$	$\frac{17}{2}^-$
412(1)	63(21)	4047.9	3635.8	$\frac{35}{2}^-$	$\frac{35}{2}^-$	$\frac{19}{2}^-$	$\frac{33}{2}^-$
441.5(3)		2885	2443.5	$\frac{21}{2}^+$	$\frac{29}{2}^+$	$\frac{21}{2}^+$	$\frac{25}{2}^+$
446.1(3)	147(62)	2546.5	2100.4	$\frac{19}{2}^-$	$\frac{25}{2}^-$	$\frac{19}{2}^-$	$\frac{21}{2}^-$
474(1)		3130	2655.9	$\frac{21}{2}^+$	$\frac{31}{2}^+$	$\frac{21}{2}^+$	$\frac{27}{2}^+$
479(1)		1527	1048.0	$\frac{1}{2}^+$	$\frac{23}{2}^+$	$\frac{1}{2}^+$	$\frac{19}{2}^+$
482.5(1)	445(105)	2796.6	2314.1	$\frac{19}{2}^-$	$\frac{27}{2}^-$	$\frac{19}{2}^-$	$\frac{23}{2}^-$

[a] Intensity inferred from intensity balances .

TABLE III – continued

E_γ (keV)	I_γ	E_i (keV)	E_f (keV)	K_i^π	J_i^π	K_f^π	J_f^π
508(1)		3393	2885	$\frac{21}{2}^+$	$\frac{33}{2}^+$	$\frac{21}{2}^+$	$\frac{29}{2}^+$
516.8(4)	103(47)	3063.3	2546.5	$\frac{19}{2}^-$	$\frac{29}{2}^-$	$\frac{19}{2}^-$	$\frac{25}{2}^-$
547.8(1)	529(104)	3344.4	2796.6	$\frac{19}{2}^-$	$\frac{31}{2}^-$	$\frac{19}{2}^-$	$\frac{27}{2}^-$
572.5(3)	58(23)	3635.8	3063.3	$\frac{19}{2}^-$	$\frac{33}{2}^-$	$\frac{19}{2}^-$	$\frac{29}{2}^-$
655(1)	33(19)	4047.9	3393	$\frac{35}{2}^-$	$\frac{35}{2}^-$	$\frac{21}{2}^+$	$\frac{33}{2}^+$
680(2)	9(5)	1343.9	662.3	$\frac{11}{2}^+$	$\frac{11}{2}^+$	$\frac{7}{2}^-$	$\frac{13}{2}^-$
694(1)	10(5)	1356	662.3	$(\frac{11}{2})$	$(\frac{11}{2})$	$\frac{7}{2}^-$	$\frac{13}{2}^-$
696.3(5)	34(17)	1691.5	995.2	$\frac{13}{2}^-$	$\frac{15}{2}^-$	$\frac{7}{2}^-$	$\frac{17}{2}^-$
703.5(1)	585(92)	4047.9	3344.4	$\frac{35}{2}^-$	$\frac{35}{2}^-$	$\frac{19}{2}^-$	$\frac{31}{2}^-$
721.3(1)	127(18)	1539.9	818.2	$\frac{13}{2}^-$	$\frac{13}{2}^-$	$\frac{7}{2}^-$	$\frac{15}{2}^-$
756.5(4)	24(8)	1751.4	995.2	$\frac{13}{2}^+$	$\frac{17}{2}^+$	$\frac{7}{2}^-$	$\frac{17}{2}^-$
767.8(3)	17(5)	1585.6	818.2	$\frac{13}{2}^+$	$\frac{15}{2}^+$	$\frac{7}{2}^-$	$\frac{15}{2}^-$
780.4(2)	26(6)	1442.7	662.3	$\frac{13}{2}^+$	$\frac{13}{2}^+$	$\frac{7}{2}^-$	$\frac{13}{2}^-$
801.3(4)	8(4)	1212.9	411.6	$\frac{9}{2}^-$	$\frac{9}{2}^-$	$\frac{7}{2}^-$	$\frac{9}{2}^-$
817.8(4)	40(18)	1343.9	526.5	$\frac{11}{2}^+$	$\frac{11}{2}^+$	$\frac{7}{2}^-$	$\frac{11}{2}^-$
830(1)	17(8)	1356	526.5	$(\frac{11}{2})$	$(\frac{11}{2})$	$\frac{7}{2}^-$	$\frac{11}{2}^-$
873.3(3)	51(17)	1691.5	818.2	$\frac{13}{2}^-$	$\frac{15}{2}^-$	$\frac{7}{2}^-$	$\frac{15}{2}^-$
877.6(7)	348(44)	1539.9	662.3	$\frac{13}{2}^-$	$\frac{13}{2}^-$	$\frac{7}{2}^-$	$\frac{13}{2}^-$
895.2(6)	40(16)	1212.9	317.7	$\frac{9}{2}^-$	$\frac{9}{2}^-$	$\frac{7}{2}^-$	$\frac{7}{2}^-$
916.1(2)	119(24)	1442.7	526.5	$\frac{13}{2}^+$	$\frac{13}{2}^+$	$\frac{7}{2}^-$	$\frac{11}{2}^-$
923.3(3)	55(11)	1585.6	662.3	$\frac{13}{2}^+$	$\frac{15}{2}^+$	$\frac{7}{2}^-$	$\frac{13}{2}^-$
932.2(4)	175(47)	1343.9	411.6	$\frac{11}{2}^+$	$\frac{11}{2}^+$	$\frac{7}{2}^-$	$\frac{9}{2}^-$
933(6)	83(21)	1751.4	818.2	$\frac{13}{2}^+$	$\frac{17}{2}^+$	$\frac{7}{2}^-$	$\frac{15}{2}^-$
945(1)	49(16)	1356	411.6	$(\frac{11}{2})$	$(\frac{11}{2})$	$\frac{7}{2}^-$	$\frac{9}{2}^-$
1013.3(1)	1103(126)	1539.9	526.5	$\frac{13}{2}^-$	$\frac{13}{2}^-$	$\frac{7}{2}^-$	$\frac{11}{2}^-$

[a] Intensity inferred from intensity balances .

TABLE III – continued

E_γ (keV)	I_γ	E_i (keV)	E_f (keV)	K_i^π J_i^π	K_f^π J_f^π
1029.2(2)	194(36)	1691.5	662.3	$\frac{13}{2}^-$ $\frac{15}{2}^-$	$\frac{7}{2}^-$ $\frac{13}{2}^-$
1128.1(2)	118(17)	1539.9	411.6	$\frac{13}{2}^-$ $\frac{13}{2}^-$	$\frac{7}{2}^-$ $\frac{9}{2}^-$
1165(1)	10(6)	1691.5	526.5	$\frac{13}{2}^-$ $\frac{15}{2}^-$	$\frac{7}{2}^-$ $\frac{11}{2}^-$

[a] Intensity inferred from intensity balances .

V. CONFIGURATION ASSIGNMENTS, DECAY HINDRANCES AND BAND PROPERTIES

The structure of these odd-A nuclei is expected to be similar to that of the neighboring even-even core nuclei, but with the unpaired proton coupled to the n-quasiparticle structures (where n = 0, 2, 4, 6...). Comparisons with the neighboring erbium, ytterbium and lutetium isotones, therefore, play a role in the configuration assignments.

The configuration of a strongly coupled rotational band is reflected in its in-band decay properties, such as the competition between E2 crossover and M1 cascade transitions, which can be examined via the γ-ray intensity branching ratio, given by

$$\lambda = \frac{I_\gamma(J \to J-2)}{I_\gamma(J \to J-1)}. \tag{1}$$

Within the rotational model, it is possible to extract the $E2/M1$ mixing ratios, δ, for the $J \to (J-1)$ transition, and the $(g_K - g_R)/Q_0$ ratio from the observed branching ratio, λ, using the relations

$$\frac{1}{\delta^2} = \frac{1}{\lambda}\left[\frac{E_\gamma(J \to J-2)}{E_\gamma(J \to J-1)}\right]^5 \frac{< JK20 \mid J-2K >^2}{< JK20 \mid J-1K >^2} - 1, \tag{2}$$

and

$$\frac{g_K - g_R}{Q_0} = 0.933 \times \frac{E_\gamma(J \to J-1)}{(\sqrt{J^2-1})\delta}. \tag{3}$$

The in-band properties for measured rotational bands in ^{173}Tm and ^{175}Tm are presented in Tables IV and V. Table VI compares (where available) experimentally measured $|g_K - g_R|$ values to empirical predictions for ^{173}Tm and ^{175}Tm.

TABLE IV: In-band decay properties for rotational bands in ^{173}Tm.

J^π	$E_\gamma(M1)$	$E_\gamma(E2)$	λ	$\lvert\delta\rvert$	$\lvert g_K\text{-}g_R\rvert^a$
$7/2^-$	**318 keV**				
$11/2^-$	114.9	208.7	0.09(2)	0.15(3)	0.99^{+14}_{-10}
$13/2^-$	135.7	250.5	0.19(3)	0.14(2)	1.04^{+10}_{-7}
$15/2^-$	155.9	291.5	0.36(6)	0.15(2)	0.98^{+10}_{-7}
$17/2^-$	176.9	332.9	0.63(22)	0.16(6)	0.90^{+22}_{-13}
$19/2^-$	196	373	0.67(20)[b]	0.14(4)	1.04^{+20}_{-13}
$13/2^+$	**1443 keV**				
$17/2^+$	165.8	308.7	0.29(5)	0.39(7)	0.35^{+4}_{-3}
$13/2^-$	**1540 keV**				
$17/2^-$	170.8	322.2	0.18(2)	0.29(3)	0.49^{+3}_{-3}
$19/2^-$	**1906 keV**				
$23/2^-$	213.7	408.4	1.3(2)	2.09(38)	0.06^{+3}_{-4}
$25/2^-$	232.4	446.1	3.2(16)	4.3(22)	$0.03^{+10}_{-(nd)}$[c]
$27/2^-$	250.1	482.5	5.1(11)	3.67(82)	$0.03^{+4}_{-(nd)}$[c]
$29/2^-$	267	516.8	6.8(49)	2.8(21)	$0.05^{+18}_{-(nd)}$[c]
$31/2^-$	281	547.8	9.3(27)	3.11(91)	$0.04^{+5}_{-(nd)}$[c]
$21/2^+$	**2061 keV**				
$25/2^+$	197.8	382.4	1.01(29)[b]	1.41(40)	0.08^{+4}_{-3}
$27/2^+$	212	410.1	2.76(123)[b]	2.7(12)	$0.04^{+7}_{-(nd)}$[c]
$29/2^+$	229	441.5	3.64(227)[b]	1.8(11)	$0.06^{+11}_{-(nd)}$[c]

[a] Assuming $Q_0 = 7.4(3)$ eb [26].

[b] Branching ratio deduced from in-beam intensities.

[c] nd: Not defined.

Figure 17 presents the net rotational alignment for bands observed in ^{173}Tm and ^{175}Tm. In both plots, reference parameters are chosen so that the average alignment for the two signatures of the $1/2^+[411]$ band is approximately zero. This requirement is equivalent to subtracting a reference representing the core contribution to the alignment. The $7/2^-[523]$

TABLE V: In-band decay properties for rotational bands in ^{175}Tm.

J^π	$E_\gamma(M1)$	$E_\gamma(E2)$	λ	$\lvert\delta\rvert$	$\lvert g_K\text{-}g_R\rvert^a$
7/2$^-$	**440 keV**				
11/2$^-$	114.1	206.2	0.11(2)	0.17(3)	0.86^{+9}_{-7}
13/2$^-$	136.8	250.9	0.25(4)	0.16(2)	0.88^{+8}_{-6}
15/2$^-$	158.6	295.4	0.47(13)	0.17(5)	0.85^{+15}_{-10}
17/2$^-$	181.6	340.2	0.66(15)^b	0.17(4)	0.88^{+12}_{-9}
19/2$^-$	200.5	382.2	0.69(22)^b	0.14(4)	1.03^{+22}_{-14}
17/2$^-$	**1005 keV**				
21/2$^-$	213.4	404.6	0.15(2)	0.31(4)	0.45^{+4}_{-3}
23/2$^-$	235.1	448.5	0.32(14)^b	0.30(13)	0.46^{+17}_{-8}
25/2$^-$	255.5	490.6	0.47(43)^b	0.29(26)	0.48^{+43}_{-15}
27/2$^-$	276	532	0.36(16)^b	0.21(10)	0.67^{+24}_{-12}

^{a}Taking Q_0 = 7.3(2) eb [27].

^{b}Branching ratio deduced from in-beam intensities.

bands in both nuclei exhibit a slight signature splitting at higher spin as expected for a member of the $h_{11/2}$ proton multiplet since significant Coriolis mixing is present.

A. The 7/2$^-$[523] Nilsson orbital

The 7/2$^-$[523] state is the lowest-lying intrinsic excitation in ^{171}Tm, ^{173}Tm and ^{175}Tm. The state is isomeric, decaying primarily via $E1$ transitions to the $J^\pi = 5/2^+$ and $7/2^+$ members of the 1/2$^+$[411] rotational band in each isotope. The hindrance values of decay branches from the 7/2$^-$[523] isomer in ^{175}Tm are given in Table VII, while those for ^{173}Tm are listed in Table VIII. $E1$ transitions are often intrinsically hindered relative to Weisskopf estimates [34]. To account for this, Tables VII and VIII include corrected $E1$ reduced hindrances (in italics) that assume a somewhat arbitrary reduction factor of 10^4 for the hindrance values. In ^{173}Tm, only the $E1$ transitions are observed, with reduced hindrance f_ν values that are very large. A limit is given for the unobserved 315-keV, $M2$ transition that also implies a large hindrance value. The reduced hindrances of the equivalent $E1$

TABLE VI: Comparison of experimental $|g_K - g_R|$ and predicted $g_K - g_R$ values for expected configurations in ^{173}Tm and ^{175}Tm.

K^π	Configuration			$g_K - g_R$ [a]	$\lvert g_K\text{-}g_R\rvert$
	ν		π	predicted	measured
^{173}Tm					
$7/2^-$			$7/2^-[523]$	+1.01	0.99(10)
$11/2^+$	$5/2^-[512]$	$7/2^-[514]$	$\downarrow 1/2^+[411]$	-0.17(8)	
$13/2^+$	$5/2^-[512]$	$7/2^-[514]$	$\uparrow 1/2^+[411]$	-0.44(7)	0.35(4)
$13/2^-$	$7/2^+[633]$	$7/2^-[514]$	$\downarrow 1/2^+[411]$	-0.10(8)	0.49(3) [b]
$13/2^-$	$5/2^-[512]$	$9/2^+[624]$	$\downarrow 1/2^+[411]$	-0.48(9)	
$15/2^-$	$7/2^+[633]$	$7/2^-[514]$	$\uparrow 1/2^+[411]$	-0.34(7)	-
$19/2^-$	$5/2^-[512]$	$7/2^-[514]$	$7/2^-[523]$	0.14(8)	0.04(3)
$21/2^+$	$7/2^+[633]$	$7/2^-[514]$	$7/2^-[523]$	0.16(8)	0.06(4)
$21/2^+$	$5/2^-[512]$	$9/2^+[624]$	$7/2^-[523]$	-0.08(8)	
$35/2^-$	$7/2^+[633]$	$5/2^-[512]$	$7/2^-[523]$	-0.14(7)	-
	$7/2^-[514]$	$9/2^+[624]$			
^{175}Tm					
$7/2^-$			$7/2^-[523]$	+1.01	0.88(9)
$15/2^-$	$7/2^-[514]$	$9/2^+[624]$	$\downarrow 1/2^+[411]$	-0.19(8)	-
$17/2^-$	$7/2^-[514]$	$9/2^+[624]$	$\uparrow 1/2^+[411]$	-0.39(7)	0.46(6)
$23/2^+$	$7/2^-[514]$	$9/2^+[624]$	$7/2^-[411]$	0.07(8)	-

[a] g_Ω from various empirical measurements [20, 22, 28–32], g_R from [33] .

[b] See text for a discussion of the 1540-keV, $13/2^-$ state.

transitions in ^{175}Tm are within the $f_\nu \sim$ 30-200 range expected for normal K-forbidden transitions [35, 36]. The hindrance for the 440-keV, $M2$ transition is, however, quite large.

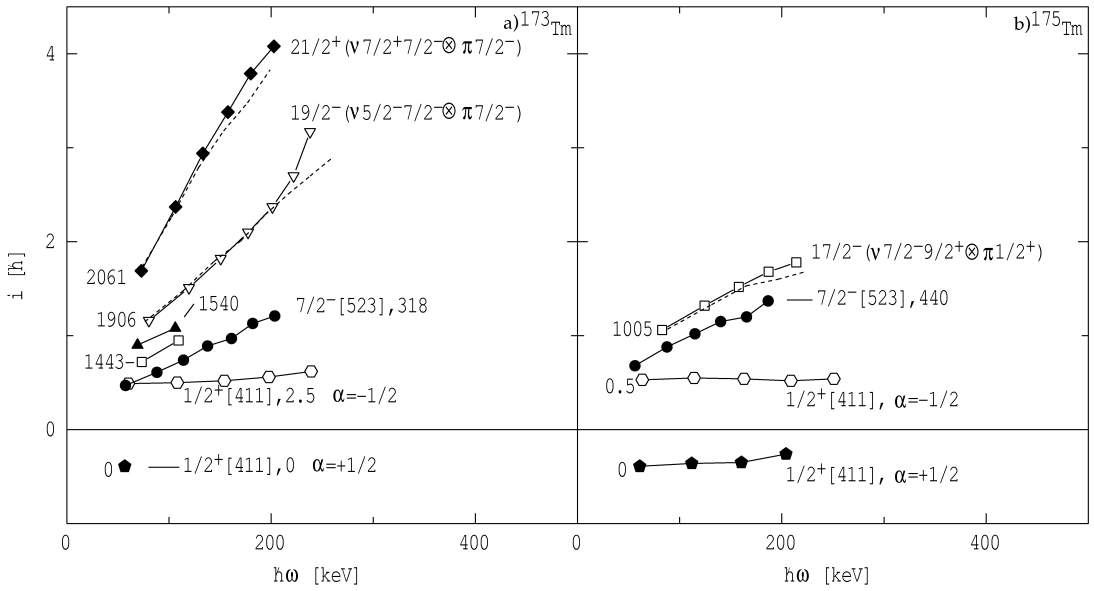

FIG. 17: Net rotational alignment in ^{173}Tm and ^{175}Tm. A reference with Harris parameters $\Im_0 = 40.9\ \hbar^2/MeV$ and $\Im_1 = 42.7\ \hbar^4/MeV^3$ for ^{173}Tm, and $\Im_0 = 38.0\ \hbar^2/MeV$ and $\Im_1 = 57.5\ \hbar^4/MeV^3$ for ^{175}Tm has been subtracted from the observed total alignments. Dashed lines are the sum of empirical neutron and proton alignments that make up the indicated multi-quasiparticle configuration (see the text).

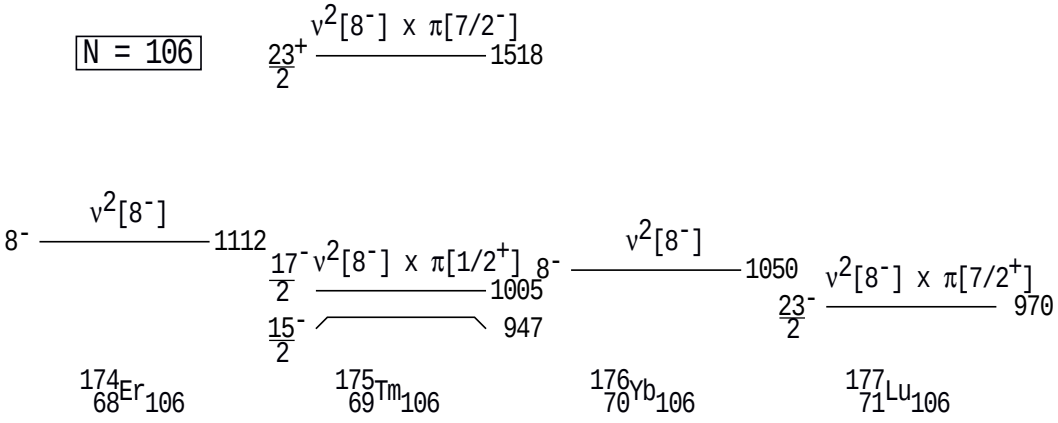

FIG. 18: Multi-quasiparticle states in the N = 106 isotones. Configuration assignments (with abbreviated labels) in ^{175}Tm are given on the basis of the expected couplings to the unpaired proton of two-quasineutron states seen in the neighboring even-even isotones.

B. Three-quasiparticle states in ^{175}Tm

1. 15/2$^-$ and 17/2$^-$ states at 947 and 1005 keV

The low-lying, $K^\pi = 8^-$ isomer constructed from the $\nu 7/2^-[514]9/2^+[624]$ neutron configuration is well known in the N = 106 isotones (at 1112 keV in ^{174}Er [3, 4] and 1050 keV in ^{176}Yb [37]). In ^{177}Lu [39], the same neutron configuration couples to the ground state $7/2^+[404]$ proton, to give a $K^\pi = 23/2^-$ isomer at 970 keV. It seems reasonable to presume that the $15/2^-$ and $17/2^-$ states in ^{175}Tm are associated with the same $\nu^2[8^-]$ configuration, coupled parallel and anti-parallel to the $1/2^+[411]$ ground state proton, as depicted in Fig. 18.

Table VI shows good agreement between the experimental and predicted $g_K - g_R$ values for the $17/2^-$ band ($\pm 0.46(6)$ and $-0.39(7)$, respectively), lending strong support to the assignment.

A reasonably large rotational alignment is associated with the $17/2^-$ band, as indicated in Fig. 17. This is consistent with the presence of an $i_{13/2}$ neutron component in the configuration. Since the $1/2^+[411]$ proton should contribute very little rotational alignment, the $17/2^-$ band alignment can be compared directly to the alignment for the $\nu 7/2^-[514]9/2^+[624]$, 8^- band in ^{176}Yb [38, 40] (with a reference appropriate for the ground state band in ^{176}Yb) as indicated by the dotted line that matches the $17/2^-$ band alignment in Fig. 17. The good agreement gives further support to a $\nu 7/2^-[514]9/2^+[624] \otimes \pi 1/2^+[411]$ configuration assignment for the $17/2^-$ state, as well as independent support for the rotational band placed on the (long-lived) 8^- isomer in ^{176}Yb.

The transition strengths and hindrances for the 947- and 1518-keV isomers in ^{175}Tm are given in Table VII. For decays from the $15/2^-$ isomer, the reduced hindrances are low, in particular the value of $f_\nu = 8(1)$ for the 301-keV, $E2$ transition. These hindrances will be discussed below in terms of state mixing. The 5.2-keV, $M1$ γ ray from the $15/2^-$ isomer is unobserved. Therefore, its intensity was inferred from the total intensity de-exciting the 942-keV level which it feeds, assuming a pure $M1$ character. Since even a small $E2/M1$ mixing ratio would significantly increase the conversion coefficient for this 5.2-keV transition, the value of I_γ is an upper limit, and the corresponding reduced hindrance value a lower limit.

2. 23/2$^+$ isomer at 1518 keV

The energy gap between the 15/2$^-$, 17/2$^-$ doublet and the 23/2$^+$ isomer is of the order of 500 keV, comparable to the 440-keV energy gap between the 1/2$^+$ ground state and the 7/2$^-$ isomer. The implication of Fig. 18 is that the $K^\pi = 23/2^+ \rightarrow K^\pi = 17/2^-$ decays are the analogue of the 7/2$^-$[523] $\rightarrow$ 1/2$^+$[411] ones, but with the single proton coupled to the ν7/2$^-$[514]9/2$^+$[624] neutron configuration.

Reduced hindrance values for the decays from the 1518-keV, 23/2$^+$ isomer are given in Table VII. The 513-keV, $E3$ transition is an allowed one, but has $F_W = 33(29)$. The reduced hindrance for the 108-keV, $E1$ transition is within the usual $f_\nu \sim$ 30-200 range for K-forbidden transitions (after accounting for an $E1$ hindrance reduction factor of 10^4). The 322-keV, $M2$ transition has a large reduced hindrance of $f_\nu = 1.9(13)\times10^3$. The hindrances for decays from the 23/2$^+$ isomer seem to be consistent with the 7/2$^-$[523] $\rightarrow$ 1/2$^+$[411] proton change (c.f. the similar reduced hindrances for the $E1$ and $M2$ decays from the 7/2$^-$[523] isomer). They, therefore, support a ν7/2$^-$[514]9/2$^+$[624]$\otimes\pi$7/2$^-$[523] configuration assignment for the 23/2$^+$ isomer.

C. Three and five-quasiparticle states in ^{173}Tm

The large number of high-K, multi-quasiparticle states observed between 1 and 2 MeV excitation energy in ^{173}Tm (see Fig. 10), can be attributed to the 5/2$^-$, 7/2$^-$, 7/2$^+$ and 9/2$^+$ neutron orbitals, all lying near the Fermi surface at N = 104.

The even-even neighbors of ^{173}Tm are ^{172}Er [3, 41] and ^{174}Yb [5]. They contain ν5/2$^-$[512]$\otimes$7/2$^-$[514], $K^\pi = 6^+$ isomers, at 1501 and 1518 keV, respectively. Both nuclei also exhibit ν7/2$^+$[633]$\otimes$7/2$^-$[514], $K^\pi = 7^-$ isomers (1792 keV in ^{172}Er and 1765 keV in ^{174}Yb). The studies of ^{174}Yb also revealed a ν5/2$^-$[512]7/2$^+$[633] 7/2$^-$[514]9/2$^+$[624], $K^\pi = 14^+$ isomer at 3699 keV [5].

The intrinsic states observed in ^{173}Tm, including likely configuration assignments, are compared to the equivalent states in the neighboring isotones in Fig. 19.

TABLE VII: Transition strengths (B(σL)), hindrances (F_W) and reduced hindrances (f_ν) for decays from the $7/2^-$, $15/2^-$ and $23/2^+$ isomers in ^{175}Tm.

E_γ (keV)	I_γ relative	σL	α_T	B(σL)[a]	F_W	ν	f_ν [b]
$7/2^-$ (440 keV, τ=460(50) ns)							
87	13(9)	$E1$	0.481	$1.9(13)\times10^{-8}$	$1.1(8)\times10^{8}$	2	$1.0(4)\times10^{4}$; *103(40)*
311	743(82)	$E1$	0.018	$2.4(4)\times10^{-8}$	$8.5(15)\times10^{7}$	2	$9.2(8)\times10^{3}$; *92(8)*
313	553(61)	$E1$	0.017	$1.7(3)\times10^{-8}$	$1.2(2)\times10^{8}$	2	$1.1(1)\times10^{4}$; *108(10)*
440	13(8)	$M2$	0.176	0.09(6)	578(364)	1	578(364)
$15/2^-$ (947 keV, τ=64(3) ns)							
5.2	<0.13[c]	($M1$)	701[c]	$<6.2\times10^{-4}$	>2906	3	>14
163.8	566(35)	$M1$	0.763	$8.6(10)\times10^{-5}$	$2.1(3)\times10^{4}$	3	28(1)
300.6	255(18)	$E2$	0.071	0.99(12)	57.6(72)	2	8(1)
$23/2^+$ (1518 keV, τ=30(20) μs)							
108.3	1000(56)	$E1$	0.270	$1.2(8)\times10^{-8}$	$1.7(11)\times10^{8}$	2	$1.3(5)\times10^{4}$; *129(45)*
321.7	53(10)	$M2$	0.474	0.03(2)	$1.9(13)\times10^{3}$	1	$1.9(13)\times10^{3}$
513	12(7)	$E3$	0.047	55(49)	33(29)	0	-

[a] B(EL) units are (e^2fm^{2L}) and B(ML) units are ($\mu_N^2 fm^{2L-2}$).

[b] Values in italics include an additional factor of 10^4 in the expected single-particle hindrance for $E1$ transitions (see text).

[c] I_γ for the unobserved, 5.2-keV transition is estimated from the sum of total intensities of 159- and 295-keV γ rays and assumes pure $M1$ multipolarity (see text for details).

1. *11/2$^+$ and 13/2$^+$ states at 1344 keV and 1443 keV*

Figure 19 implies the presence of a low-lying $\nu 5/2^-[512]7/2^-[514]\otimes\pi 1/2^+[411]$ configuration in ^{173}Tm. It is likely that the $11/2^+$, 1344- and $13/2^+$, 1443-keV states are associated with the anti-parallel ($-1/2^+[411]$) and parallel ($+1/2^+[411]$) proton couplings of this configuration, respectively. The $|g_K - g_R|$ value in Table VI for the $13/2^+$ band is consistent with such an assignment. The $7/2^-[514]\otimes 1/2^+[411]$ and $5/2^-[512]\otimes 1/2^+[411]$ residual in-

TABLE VIII: Transition strengths (B(σL)), hindrances (F_W) and reduced hindrances (f_ν) for decays from isomers in ^{173}Tm. Two possible assignments: $35/2^-$ and $35/2^+$ are shown for the isomer at 4048 keV.

E_γ (keV)	I_γ relative	σL	α_T	B(σL)[a]	F_W	ν	f_ν [b]
7/2$^-$ (318 keV, τ=15(3) μs)							
193	516(50)	$E1$	0.059	$2.7(7)\times10^{-9}$	$7.3(18)\times10^{8}$	2	$2.7(3)\times10^{4}$; *270(33)*
199	532(50)	$E1$	0.054	$2.6(6)\times10^{-9}$	$7.8(19)\times10^{8}$	2	$2.8(3)\times10^{4}$; *278(34)*
315	<20	$M2$	0.508	$<3\times10^{-2}$	$>1.8\times10^{3}$	1	$>1.8\times10^{3}$
19/2$^-$ (1906 keV, τ=360(100) ns)							
43.4	272(68)[c]	$M1$	5.77	$2.0(8)\times10^{-4}$	$8.8(34)\times10^{3}$	2	94(19)
154.3	440(44)	$E1$	0.106	$8.1(25)\times10^{-8}$	$2.5(8)\times10^{7}$	2	$5.0(8)\times10^{3}$; *50(8)*
214.3	102(15)	$E2$	0.207	0.20(7)	288(95)	1	288(95)
124	9(5)	$E2$	1.377	0.27(17)	212(133)	0	-
35/2$^-$ (4048 keV, τ=175(40) ns)							
412	63(21)	$M1$	0.063	$4.2(17)\times10^{-7}$	$4.2(17)\times10^{6}$	7	9(1)
655	33(19)	$E1$	0.0033	$6.1(38)\times10^{-10}$	$3.3(20)\times10^{9}$	6	38(4); *8(1)*
703.5	585(92)	$E2$	0.0075	$2.3(6)\times10^{-2}$	$2.5(7)\times10^{3}$	6	4(1)

[a] B(EL) units are (e^2fm^{2L}) and B(ML) units are ($\mu_N^2 fm^{2L-2}$).

[b] Values in italics include an additional factor of 10^4 in the expected single-particle hindrance for $E1$ transitions (see text).

[c] Inferred from the intensity balance with the 171- (δ(171 keV) = 0.29(3)) and 322-keV γ rays, due to the difficulty of accurately measuring the intensity for the 43-keV line.

teractions predict that the $11/2^+$ coupling is energetically favored by 116 keV over the $13/2^+$ coupling. This is in approximate agreement with the 99-keV difference observed experimentally. The alignment for the 1443-keV, $13/2^+$ band, illustrated in Fig. 17, is surprisingly large, considering the absence of either an $h_{11/2}$ proton or an $i_{13/2}$ neutron.

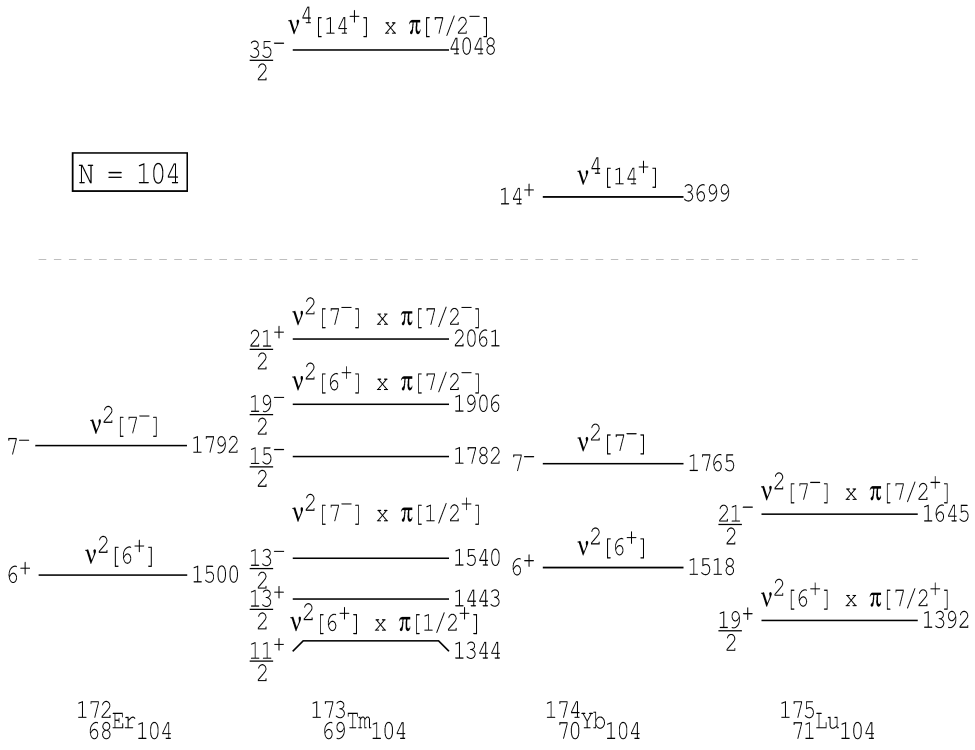

FIG. 19: Multi-quasiparticle states in the N = 104 isotones. Configuration assignments (with abbreviated labels) in ^{173}Tm are proposed on the basis of the expected couplings to the unpaired proton of 2- and 4-quasineutron states seen in the neighboring even-even isotones. The dotted line signifies a break in the energy scale to display the higher-seniority isomers.

2. 13/2$^-$, 15/2$^-$ and 17/2$^-$ states at 1540, 1692 and 1862 keV and the (15/2$^-$) state at (1782 keV)

The reduced hindrance values for the 43-keV, $M1$ and 214-keV, $E2$ branches from the 19/2$^-$ isomer (Table VIII) are consistent with the 1692- and 1862-keV states being the 15/2$^-$ and 17/2$^-$ members of a band built on the $K^\pi = 13/2^-$ level at 1540 keV. Figure 19 would suggest a $\nu 7/2^+[633]7/2^-[514]\otimes\pi{-}1/2^+[411]$ configuration assignment for the 13/2$^-$ state. However, Table VI indicates that the $|g_K{-}g_R|$ value deduced from the 171/322-keV branching ratio is inconsistent with the prediction for this configuration.

One possible explanation is that the 15/2$^-$, 1692-keV level is in fact not a band member, but corresponds instead to the $\nu 7/2^+[633]7/2^-[514]\otimes\pi{+}1/2^+[411]$ coupling from the same configuration. This would explain the disagreement of the $|g_K{-}g_R|$ value, as well as the

observation of strongly competing, K-forbidden, inter-band transitions from the 1692-keV level to the $7/2^-[523]$ band. However, assuming that the $17/2^-$ state is then in a band built on a $15/2^-$ intrinsic state at 1692 keV, the 43-keV transition from the 1906-keV isomer would have a very large reduced hindrance of $f_\nu = 8.8(33)\times10^3$.

A $13/2^-$ state can also be constructed from the $\nu 5/2^-[512]9/2^+[624] \otimes \pi - 1/2^+[411]$ configuration. This gives a predicted $(g_K - g_R) = -0.48(9)$, in much better agreement with experiment. However, the multi-quasiparticle calculation (section VI) predicts that this state should lie more than 200 keV higher than the favored configuration assignment. Given the predicted close proximity of these two states, it is possible that the $13/2^-$ level at 1540 keV represents a mixture of the two configurations.

The alignments in Fig. 17 indicate that the $13/2^-$, 1540-keV state has a reasonably large rotational alignment. This is consistent with the presence of an $i_{13/2}$ neutron in its configuration.

The $(15/2^-)$ state at 1782 keV may have an alternative energy placement of 1664 keV (if the order of the 124- and 242-keV transitions is reversed). It is a candidate for the $\nu 7/2^+[633]7/2^-[514] \otimes \pi + 1/2^+[411]$ configuration, as implied by Fig. 19.

3. $19/2^-$ isomer at 1906 keV

A $19/2^-$ state is expected to be formed from the $\nu 5/2^-[512]7/2^-[514]$ configuration (see Fig. 19) coupled to the $7/2^-[523]$ proton excitation. The 1906-keV, $19/2^-$ isomer lies at the expected energy, and reasonable agreement is seen between the experimental $|g_K - g_R|$ value and that predicted for this configuration in Table VI.

The rotational alignment of the $19/2^-$ band is plotted in Fig. 17. The nearby dotted line shows the expected alignment for this configuration as obtained from the sum of the $7/2^-[523]$ alignment and that of the $\nu 5/2^-[512]7/2^-[514]$, 6^+ band in ^{174}Yb [5] (with a reference appropriate for the ^{174}Yb ground state band). The excellent agreement between the two curves gives additional confidence in this configuration assignment, and suggests that, in this case, the neutron and proton components of the rotational alignments are approximately additive, provided that appropriate references are chosen in each case. The sudden increase in alignment at the top of the observed $19/2^-$ band is probably an indication of the beginning of a backbend [42] and will be discussed below.

Table VIII presents hindrances for decay branches from the 1906-keV isomer. Reasonable reduced hindrances are seen for the 43-, 154- and 214-keV branches with the present spin and parity assignments. The $f_\nu = 50(8)$ value for the 154-keV transition is in contrast to the large reduced hindrances of the 193- and 199-keV, $E1$ transitions from the $7/2^-$ isomer at 318 keV, that should represent the one-quasiparticle analogue of the 154-keV transition. For the decay to the 1782-keV (or 1664-keV) level, the transition can have an energy of either 124 or 242 keV and can be of $M1$ or $E2$ multipolarity so that there are four possible hindrance values. Of the four possibilities, a 124-keV, $E2$ transition appears to be the most reasonable (the alternative assignments imply allowed transitions with hindrance values, $F_W \geq 3.7\times10^3$). However, the $15/2^-$ spin/parity and 1782-keV energy assignments for this state remain tentative.

4. $21/2^+$ state at 2061 keV

The experimental $|g_K - g_R|$ value for the $21/2^+$ band is in good agreement with that expected for the $\nu 7/2^+[633]7/2^-[514] \otimes \pi 7/2^-[523]$ configuration (Table VI). However, it is also consistent with the the $|g_K - g_R|$ value for the $\nu 9/2^+[624]\ 5/2^-[512] \otimes \pi 7/2^-[523]$ configuration, which could also be low lying.

Since both configurations contain a $h_{11/2}$ proton and an $i_{13/2}$ neutron, both are consistent with the large alignment observed in Fig. 17. The dotted line which closely follows the $21/2^+$ alignment, is a sum of the $7/2^-[523]$ alignment with that of the $\nu 7/2^+[633]7/2^-[514]$, 7^- band in ^{174}Yb [5] (with a reference appropriate for the ^{174}Yb ground state band). The agreement is consistent with an assignment to the $\nu 7/2^+[633]7/2^-[514] \otimes \pi 7/2^-[523]$ configuration.

5. $35/2^-$ isomer at 4048 keV

The absence of a rotational band associated with this state precludes a $g_K - g_R$ measurement so that no firm configuration assignment can be proposed on this basis. Nevertheless, comparison with the 14^+ isomer in ^{174}Yb (Fig. 19), but with the addition of a $7/2^-[523]$ proton gives the expectation of a $35/2^-$ state at approximately 4017 keV (neglecting residual interactions and taking $E_x(7/2^-[523]) = 318$ keV).

A $\nu 7/2^+[633]7/2^-[514]9/2^+[624]5/2^-[512]\otimes\pi 7/2^-[523]$ configuration assignment, therefore, seems very likely for the $35/2^-$, 4048-keV isomer.

The reduced hindrance values for all three branches from the $35/2^-$ isomer (Table VIII) are low, and will be discussed below.

VI. MULTI-QUASIPARTICLE CALCULATIONS

The multi-quasiparticle calculations employed here have been described in connection with several investigations in this mass region (see Refs. [2, 5, 7, 32], for example). They use single-particle energies from a Nilsson calculation, and the Lipkin-Nogami formalism (plus pair-blocking) for calculating pairing correlations. The calculations were performed systematically for the thulium isotopes between A = 171 and A = 175, although the present paper will focus on ^{173}Tm and ^{175}Tm only.

The Nilsson calculation parameters were adopted from Ref. [43] while deformation parameters for thulium isotopes from A =171-175 were taken from Ref. [44]. Single-particle Nilsson orbitals were generated for the N = 4, 5 and 6 proton and neutron oscillator shells (a total of 128 states). For simplicity, a fixed, configuration independent deformation is used for all Nilsson orbitals. (Configuration-dependent deformations calculated for single proton states by Nazarewicz *et al.* [45] suggest only small differences in deformation between, for example, the $1/2^+[411]$ and $7/2^-[523]$ orbitals within a given nucleus).

After calculation with the initial set of Nilsson energies, the neutron and proton orbitals near the Fermi surface were adjusted to ensure that the multi-quasiparticle calculation approximately reproduced the experimental one-quasiparticle energies for protons in the odd-A thulium isotopes, and, in the odd-A erbium and ytterbium isotopes for neutrons.

Pairing strength parameters of $G_\nu = 18.0/A$ MeV and $G_\pi = 20.8/A$ MeV were used for neutrons and protons, respectively. These were chosen to approximately reproduce the odd-even mass differences in the neutron and proton pairing gaps, and to be consistent with previous calculations for tantalum, lutetium and ytterbium nuclei in this region [2, 5, 7, 32].

The multi-quasiparticle energies obtained by combining the calculated multi-quasiproton and multi-quasineutron components are subsequently corrected for the residual nucleon-nucleon interactions. These are taken from the present work (where applicable), from Ref. [10] and from Kondev [46]. For multi-quasiparticle states, a sum of the individual two-

quasiparticle residual interactions was used following the generalized form given by Jain *et al.* [47]. Strictly speaking, each multi-quasiparticle configuration should also be corrected for perturbations from rotational and Coriolis shifts, but these are usually relatively minor and have been neglected here [46].

The energies of the calculated multi-quasiparticle configurations and experimental states are compared in Table IX and Table X for ^{173}Tm and ^{175}Tm, respectively, as well as in Fig. 20. Only those states calculated within reasonable proximity to the nominal yrast line are included.

TABLE IX: Calculated multi-quasiparticle states compared to experiment for ^{173}Tm.

K^π	Configuration[a]		E_{qp}	E_{res}	E_{calc}	E_{exp}
	ν	π	(keV)	(keV)	(keV)	(keV)
$1/2^+$		$1/2^+$	0	0	0	0
$3/2^+$		$3/2^+$	640	0	640	
$7/2^-$		$7/2^-$	320	0	320	318
$7/2^+$		$7/2^+$	822	0	822	
$9/2^-$		$9/2^-$	1213	0	1213	1213
$11/2^+$	$5/2^-$, $7/2^-$	$1/2^+$	1540	-188	1352	1344
$13/2^+$	$5/2^-$, $7/2^-$	$1/2^+$	1540	-72	1472	1443
$13/2^-$	$7/2^+$, $7/2^-$	$1/2^+$	1763	-108	1655	1540
$13/2^-$	$5/2^-$, $9/2^+$	$1/2^+$	1893	-10	1883	
$15/2^-$	$7/2^+$, $7/2^-$	$1/2^+$	1763	-78	1685	(1782)
$15/2^-$	$5/2^-$, $9/2^+$	$1/2^+$	1893	$+378$	2271	
$15/2^-$		$1/2^+$, $7/2^-$, $7/2^+$	2256	-65	2191	
$15/2^+$	$7/2^+$, $9/2^+$	$1/2^+$	2101	$+51$	2152	
$17/2^+$	$7/2^+$, $9/2^+$	$1/2^+$	2101	$+349$	2450	
$17/2^-$	$7/2^-$, $9/2^+$	$1/2^+$	2262	-69	2193	

[a] Configurations: (ν) $1/2^-$: $1/2^-[521]$, $7/2^-$: $7/2^-[514]$, $7/2^+$: $7/2^+[633]$, $5/2^-$: $5/2^-[512]$, $9/2^+$: $9/2^+[624]$, $3/2^-$: $3/2^-[512]$. (π) $1/2^+$: $1/2^+[411]$, $7/2^-$: $7/2^-[523]$, $3/2^+$: $3/2^+[411]$, $7/2^+$: $7/2^+[404]$, $9/2^-$: $9/2^-[514]$.

TABLE IX – continued

K^π	Configuration[a]		E_{qp}	E_{res}	E_{calc}	E_{exp}
	ν	π	(keV)	(keV)	(keV)	(keV)
$19/2^-$	$5/2^-$, $7/2^-$	$7/2^-$	1860	−177	1683	1906
$19/2^+$	$5/2^-$, $7/2^-$	$7/2^+$	2362	−200	2162	
$21/2^+$	$7/2^+$, $7/2^-$	$7/2^-$	2083	−93	1990	2061
$21/2^+$	$5/2^-$, $9/2^+$	$7/2^-$	2213	+19	2232	
$21/2^-$	$7/2^+$, $7/2^-$	$7/2^+$	2585	−158	2428	
$21/2^-$	$5/2^-$, $7/2^-$	$9/2^-$	2752	−162	2590	
$23/2^-$	$7/2^+$, $9/2^+$	$7/2^-$	2421	+85	2506	
$23/2^+$	$7/2^-$, $9/2^+$	$7/2^-$	2582	−122	2460	
$23/2^-$	$7/2^-$, $9/2^+$	$7/2^+$	3084	−156	2928	
$25/2^+$	$7/2^-$, $9/2^+$	$9/2^-$	3474	−114	3360	
$25/2^-$	$7/2^+$, $9/2^+$	$9/2^-$	3313	+58	3371	
$27/2^+$	$5/2^-$, $7/2^+$, $7/2^-$, $9/2^+$	$1/2^+$	3509	+54	3563	
$27/2^-$	$5/2^-$, $7/2^-$	$1/2^+$, $7/2^-$, $7/2^+$	3796	−61	3735	
$29/2^+$	$5/2^-$, $7/2^+$, $7/2^-$, $9/2^+$	$1/2^+$	3509	+472	3981	
$29/2^+$	$7/2^+$, $7/2^-$	$1/2^+$, $7/2^+$, $7/2^-$	4019	+189	4208	
$31/2^-$	$7/2^+$, $9/2^+$	$1/2^+$, $7/2^-$, $7/2^+$	4357	+286	4643	
$31/2^-$	$7/2^+$, $7/2^-$	$1/2^+$, $7/2^-$, $9/2^-$	4399	−7	4392	
$33/2^+$	$7/2^+$, $9/2^+$	$1/2^+$, $7/2^-$, $9/2^-$	4737	+182	4918	
$35/2^-$	$5/2^-$, $7/2^+$, $7/2^-$, $9/2^+$	$7/2^-$	3829	+98	3927	4048
$35/2^+$	$5/2^-$, $7/2^+$, $7/2^-$, $9/2^+$	$7/2^+$	4331	+319	4650	
$37/2^-$	$5/2^-$, $7/2^+$, $7/2^-$, $9/2^+$	$9/2^-$	4722	+87	4809	
$39/2^+$	$7/2^+$, $9/2^+$	$7/2^+$, $7/2^-$, $9/2^-$	5860	−68	5793	
$43/2^-$	$5/2^-$, $7/2^+$, $7/2^-$, $9/2^+$	$1/2^+$, $7/2^-$, $7/2^+$	5765	+295	6060	

[a] Configurations: (ν) $1/2^-$: $1/2^-[521]$, $7/2^-$: $7/2^-[514]$, $7/2^+$: $7/2^+[633]$, $5/2^-$: $5/2^-[512]$, $9/2^+$: $9/2^+[624]$, $3/2^-$: $3/2^-[512]$. (π) $1/2^+$: $1/2^+[411]$, $7/2^-$: $7/2^-[523]$, $3/2^+$: $3/2^+[411]$, $7/2^+$: $7/2^+[404]$, $9/2^-$: $9/2^-[514]$.

TABLE X: Calculated multi-quasiparticle states compared to experiment for ^{175}Tm.

K^π	Configuration[a]		E_{qp}	E_{res}	E_{calc}	E_{exp}
	ν	π	(keV)	(keV)	(keV)	(keV)
$1/2^+$		$1/2^+$	0	0	0	0
$7/2^-$		$7/2^-$	438	0	438	440
$3/2^+$		$3/2^+$	624	0	624	611
$7/2^+$		$7/2^+$	869	0	869	
$9/2^-$		$9/2^-$	1157	0	1157	1175
$9/2^+$	$1/2^-$, $7/2^-$	$1/2^+$	1548	-193	1361	
$11/2^-$	$1/2^-$, $9/2^+$	$1/2^+$	1670	$+285$	1955	
$11/2^+$	$3/2^-$, $7/2^-$	$1/2^+$	1729	$+33$	1762	
$11/2^+$	$5/2^-$, $7/2^-$	$1/2^+$	2062	-188	1874	
$11/2^+$	$1/2^-$, $7/2^-$	$3/2^+$	2172	-173	1999	
$13/2^-$	$3/2^-$, $9/2^+$	$1/2^+$	1851	-176	1676	
$13/2^+$	$5/2^-$, $7/2^-$	$1/2^+$	2062	-68	1994	
$13/2^-$	$1/2^-$, $9/2^+$	$3/2^+$	2294	$+11$	2305	
$15/2^-$	$7/2^-$, $9/2^+$	$1/2^+$	1048	-117	931	947
$15/2^-$	$5/2^-$, $9/2^+$	$1/2^+$	1967	$+370$	2337	
$15/2^-$	$1/2^-$, $7/2^-$	$7/2^-$	1986	-281	1705	
$15/2^+$	$1/2^-$, $7/2^-$	$7/2^+$	2417	-265	2152	
$17/2^-$	$7/2^-$, $9/2^+$	$1/2^+$	1048	-69	979	1005
$17/2^+$	$1/2^-$, $9/2^+$	$7/2^-$	2108	-56	2052	
$19/2^-$	$7/2^-$, $9/2^+$	$3/2^+$	1672	-108	1565	
$19/2^+$	$3/2^-$, $9/2^+$	$7/2^-$	2289	-142	2147	
$21/2^+$	$5/2^-$, $9/2^+$	$7/2^-$	2405	$+19$	2424	

[a] Configurations: (ν) $1/2^-$: $1/2^-[510]$, $7/2^-$: $7/2^-[514]$, $7/2^+$: $7/2^+[633]$, $5/2^-$: $5/2^-[512]$, $9/2^+$: $9/2^+[624]$, $3/2^-$: $3/2^-[512]$. (π) $1/2^+$: $1/2^+[411]$, $7/2^-$: $7/2^-[523]$, $3/2^+$: $3/2^+[411]$, $7/2^+$: $7/2^+[404]$, $9/2^-$: $9/2^-[514]$.

TABLE X – continued

K^π	Configuration[a]		E_{qp}	E_{res}	E_{calc}	E_{exp}
	ν	π	(keV)	(keV)	(keV)	(keV)
$23/2^+$	$7/2^-$, $9/2^+$	$7/2^-$	1486	−119	1367	1518
$23/2^-$	$7/2^-$, $9/2^+$	$7/2^+$	1917	−156	1761	
$25/2^+$	$7/2^-$, $9/2^+$	$9/2^-$	2205	−114	2091	
$25/2^-$	$3/2^-$, $5/2^-$, $7/2^-$, $9/2^+$	$1/2^+$	3302	−144	3158	
$27/2^+$	$3/2^-$, $7/2^+$, $7/2^-$, $9/2^+$	$1/2^+$	3579	−164	3415	
$27/2^-$	$7/2^-$, $9/2^+$	$1/2^+$, $3/2^+$, $7/2^+$	3621	−190	3431	
$27/2^-$	$3/2^-$, $5/2^-$, $7/2^-$, $9/2^+$	$3/2^+$	3926	−213	3713	
$29/2^+$	$1/2^-$, $5/2^-$, $7/2^-$, $9/2^+$	$7/2^-$	3572	−181	3391	
$29/2^-$	$1/2^-$, $5/2^-$, $7/2^-$, $9/2^+$	$7/2^+$	4003	+119	4122	
$31/2^+$	$7/2^-$, $9/2^+$	$1/2^+$, $7/2^-$, $7/2^+$	3435	−224	3211	
$31/2^+$	$3/2^-$, $5/2^-$, $7/2^-$, $9/2^+$	$7/2^-$	3739	−229	3510	
$31/2^-$	$1/2^-$, $7/2^+$, $7/2^-$, $9/2^+$	$7/2^-$	3849	−16	3833	
$31/2^-$	$3/2^-$, $5/2^-$, $7/2^-$, $9/2^+$	$7/2^+$	4170	−246	3924	
$33/2^-$	$7/2^-$, $9/2^+$	$1/2^+$, $7/2^-$, $9/2^-$	3714	−17	3697	
$33/2^-$	$3/2^-$, $7/2^+$, $7/2^-$, $9/2^+$	$7/2^-$	4017	−154	3863	
$33/2^+$	$7/2^-$, $9/2^+$	$3/2^+$, $7/2^-$, $7/2^+$	4095	−366	3729	
$39/2^-$	$7/2^-$, $9/2^+$	$7/2^-$, $7/2^+$, $9/2^-$	4847	−341	4506	

[a] Configurations: (ν) $1/2^-$: $1/2^-[510]$, $7/2^-$: $7/2^-[514]$, $7/2^+$: $7/2^+[633]$, $5/2^-$: $5/2^-[512]$, $9/2^+$: $9/2^+[624]$, $3/2^-$: $3/2^-[512]$. (π) $1/2^+$: $1/2^+[411]$, $7/2^-$: $7/2^-[523]$, $3/2^+$: $3/2^+[411]$, $7/2^+$: $7/2^+[404]$, $9/2^-$: $9/2^-[514]$.

A. Comparison between experimental and calculated states

The predicted one-quasiproton energies in the odd-A nuclei do not provide a true test of the calculations since they have been adjusted to match experiment in cases where they are known. The predictions for higher-seniority configurations provide a better test, and the agreement here is usually within 150 keV of experiment.

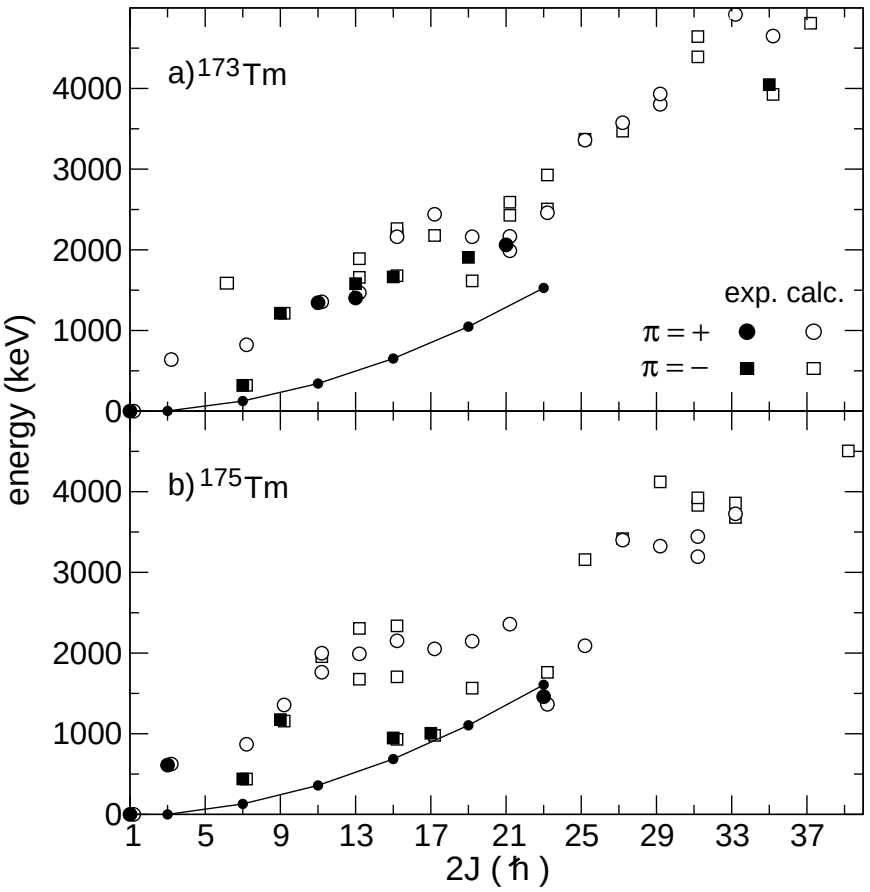

FIG. 20: Experimental and calculated single and multi-quasiparticle state energies for ^{173}Tm and ^{175}Tm. The smaller filled, joined symbols represent the $\alpha = -1/2$ signature of the $1/2^+[411]$ ground state band.

1. ^{173}Tm

The $11/2^+$ and $13/2^+$ states observed at 1344 and 1443 keV, respectively, are proposed to represent the $\nu 5/2^-[512]7/2^-[514]\otimes\pm\pi 1/2^+[411]$ configurations. They are reproduced well at 1352 and 1472 keV, respectively.

A prediction of 1655 keV for the $13/2^-$ coupling of the $\nu 7/2^+[633]$ $7/2^-[514]\otimes-\pi 1/2^+[411]$ configuration, approximately agrees with the $13/2^-$ state observed at 1540 keV.

The $15/2^-$ coupling of the $\nu 7/2^+[633]7/2^-[514]\otimes+\pi 1/2^+[411]$ configuration is predicted by the residual interactions to be 30 keV higher-lying than the $13/2^-$ coupling. Possible candidates for the parallel coupling are the $(15/2^-)$ state at 1664/1782 keV or the $15/2^-$ state at 1692 keV (the latter is, however, more likely to be the $15/2^-$ member of the $K^\pi = 13/2^-$

rotational band).

The $\nu 5/2^-[512]7/2^-[514]\otimes\pi 7/2^-[523]$ configuration is predicted 223 keV lower than the $19/2^-$ isomer at 1906 keV. No alternative $19/2^-$ configurations are predicted, and this assignment seems likely.

The 2106-keV, $21/2^+$ isomer has possible assignments as the $\nu 7/2^+[633]$ $7/2^-[514]\otimes\pi 7/2^-[523]$ or $\nu 5/2^-[512]9/2^+[624]\otimes\pi 7/2^-[523]$ configurations. The former is predicted at 1990 keV, which is within 100 keV of the experimental state and over 200 keV lower than the alternative configuration. The $\nu 5/2^-[512]7/2^+[633]7/2^-[514]9/2^+[624]\otimes\pi 7/2^-[523]$ configuration is predicted within 121 keV of the $35/2^-$ isomer at 4048 keV, in excellent agreement. No other states with comparable K values are expected to occur this low in excitation energy.

2. ^{175}Tm

The agreement between experiment and calculation for ^{175}Tm is satisfactory. The $15/2^-$ and $17/2^-$ couplings of the $\nu 7/2^-[514]9/2^+[624]\otimes \pm \pi 1/2^+[411]$ configuration are both well reproduced, falling within 30 keV of experiment. The nearest alternative states with $J = 15/2$ or $17/2$ are predicted more than 700 keV higher in energy. The $23/2^+$ isomer resulting from the $\nu 7/2^-[514]9/2^+[624]\otimes\pi 7/2^-[523]$ configuration is calculated to lie at 1367 keV, 151 keV lower than the experimental value of 1518 keV. No other $J^\pi = 21/2^+$ or $23/2^+$ states are expected below 2 MeV in excitation. Predicted low-lying five-quasiparticle states include a $31/2^+$ state calculated to lie at 3211 keV, from the $\nu 7/2^-[514]9/2^+[624]\otimes\pi 1/2^+[411]7/2^-[523]7/2^+[404]$ configuration, although the unknown energy of the $\pi 7/2^+[404]$ orbital makes this prediction rather unreliable.

3. General agreement

The agreement between experimental and calculated states for both ^{173}Tm and ^{175}Tm is typically within 150 keV, and is no worse than 250 keV for any given state. This is comparable to similar multi-quasiparticle studies in this region. For example, experimentally observed states in the nearby nuclei, ^{174}Yb [5] and ^{176}Lu [7], are reproduced to within about 200 keV in similar calculations.

VII. DISCUSSION

A. Anomalous decays from the $35/2^-$ isomer in ^{173}Tm

In ^{173}Tm, the $35/2^-$ isomer decays via 412-keV, $M1$ and 704-keV, $E2$ transitions to the $19/2^-$ band, and via a 655-keV, $E1$ transition to the $21/2^+$ band. The 412-, 704- and 655-keV transitions have reduced hindrance values of $f_\nu = 9(4)$, 4(1) and 8(1), respectively. These are all unusually small.

As was shown in Fig. 19, the $35/2^-$, $19/2^-$ and $21/2^+$ states in ^{173}Tm are the analogues of the $K^\pi = 14^+$, 6^+ and 7^- states in the even-even isotone, ^{174}Yb, obtained by adding the $7/2^-[523]$ proton component to the ^{174}Yb core. The 14^+ isomer in ^{174}Yb also exhibits decay branches with small hindrance values to the 6^+ and 7^- bands. Dracoulis *et al.* [5] ascribe these low hindrances to Coriolis mixing from the $i_{13/2}$ neutrons contained within the configuration of the 14^+ isomer, and probable chance mixing with nearby 14^+ levels at this energy (seated over 1 MeV above the yrast line).

The Coriolis mixing discussed in the ^{174}Yb case would presumably also contribute to the low reduced hindrances of transitions from the $35/2^-$ isomer in ^{173}Tm, especially since the additional $h_{11/2}$ proton will also be Coriolis mixed. For ^{173}Tm, the $35/2^-$ isomer is $\sim$600 keV above the yrast line, so the surrounding level density should be somewhat lower than that surrounding the 14^+ isomer in ^{174}Yb, and fewer $35/2^-$ states will be available for state mixing as a result.

An analogous, $K^\pi = 22^-$, six-quasiparticle isomer was recently observed in ^{176}Hf by Mukherjee *et al.* [48]. Its configuration contains the same four quasineutrons as the 14^+ (^{174}Yb) and $35/2^-$ (^{173}Tm) levels, and shows a relatively enhanced K-forbidden $E2$ decay to a $K^\pi = 14^-$ band. Mukherjee *et al.* also propose possible statistical and Coriolis mixing to account for the enhancement, but also suggest local mixing of either the 22^- isomer with the (unobserved, $\Delta E \sim 723$ keV) 22^- member of the 14^- band, or mixing of the 20^- final state with a nearby ($\Delta E = 60$ keV) 20^- level. While the latter is a special case, the former can be compared with chance mixing of the $35/2^-$ isomer and the (unobserved) $35/2^-$ member of the $K^\pi = 19/2^-$ band in ^{173}Tm. An energy separation of 111 keV between the two $35/2^-$ levels can be estimated from an extrapolation of the $19/2^-$ rotational band. A mixing amplitude of $\beta = 1.6\times10^{-3}$, and an interaction strength of $V = 0.17$ keV are deduced

in a manner similar to Refs. [6, 49]. This mixing amplitude would imply that a contribution of $\beta^2 = 2.56\times10^{-6}$ of the $K^\pi = 19/2^-$ component to the $K^\pi = 35/2^-$ wavefunction is sufficient to explain the observed strength of the 412-keV and 704-keV transitions to the $K^\pi = 19/2^-$ band. However, such mixing should also enhance the 655-keV, $E1$ transition since the $19/2^-$ admixture in the $35/2^-$ state wavefunction would give an allowed component for the $E1$ transition to the $21/2^+$ band. The transition strength for an allowed $E1$ transition between these two configurations is already known in this case, since the 155-keV, $21/2^+ \rightarrow 19/2^-$ decay corresponds to the reverse transition, with a measured B($E1$) value of $6.9^{+4.1}_{-1.8}\times10^{-6}e^2fm^2$. Taking the same B($E1$) value for the 655-keV transition, but with an amplitude of $\beta^2 = 2.56\times10^{-6}$, gives B($E1$) = $1.8^{+1.1}_{-0.5}\times10^{-11}e^2fm^2$. This value is smaller than the experimentally measured transition strength of B($E1$) = $6.1(38)\times10^{-10}e^2fm^2$ for the 655-keV transition, suggesting that, on its own, such mixing cannot fully account for the enhancement of this transition from the $35/2^-$ isomer.

It is interesting to note the similarity in the configurations of the $19/2^-$ and $35/2^-$ states, the latter having the $7/2^+[633]$ and $9/2^+[624]$ neutrons coupled to the $19/2^-$ configuration. These two $i_{13/2}$ neutrons are also partially aligned to the rotation axis, making this isomer the bandhead of a so-called Fermi-aligned or t-band [50, 51]. (In such a band, the single-particle angular momentum, j, precesses around an axis intermediate between the symmetry and rotation axes.)

The sudden increase in alignment observed at $\hbar\omega \sim 0.22$ MeV for the $19/2^-$ band in Fig. 17 suggests the beginnings of a backbend [42]. This is attributed to the introduction of rotational alignment from a pair of high-j nucleons (in this case, two $i_{13/2}$ neutrons), coupled so that $K \approx 0$. The consequent rotation-aligned sequence of states (in this case, a three-quasiparticle state coupled to the $(i_{13/2})^2$ neutrons) is then called the s-band.

The 412- and 704-keV transitions are, therefore, likely to be decays between the bandhead of the $K^\pi = 35/2^-$, t-band and the $K^\pi = 19/2^-$ s-band. The two configurations contain the same five quasiparticles, but, in the case of the $35/2^-$ isomer, the two $i_{13/2}$ neutrons are coupled parallel, and in the $19/2^-$ s-band, they are coupled anti-parallel.

B. The competition between K-forbidden $E1$ transitions and collective $E2$ and $M1$ transitions in ^{173}Tm

The $K^\pi = 13/2^+$ state at 1433-keV is proposed to be composed of the $\nu 5/2^-[512]7/2^-[514]$ $\otimes$ $\pi{+}1/2^+[411]$ configuration. It has rotational members at 1586-keV and 1751-keV, both of which show $\nu = 2$, $E1$ branches to the $7/2^-[523]$ rotational band.

Only lifetime limits of $\tau < 5$ ns were obtained for each level, however transition strengths can be deduced indirectly for the K-forbidden decay branches by scaling the observed γ-ray branches to the partial γ-ray widths of the in-band $E2$ or $M1$ transitions (calculated assuming the rotational model). For the 309-keV, $E2$ decay from the 1751-keV level, a γ-ray width of $4.2(3) \times 10^{-6}$ eV was deduced. This leads to implied widths of $1.9(8) \times 10^{-6}$ eV and $6.5(22) \times 10^{-6}$ eV for the 757- and 933-keV transitions, respectively. These widths correspond to strengths of $2.1(8) \times 10^{-6}$ $W.u.$ and $3.8(13) \times 10^{-6}$ $W.u.$ for the two transitions. For the 1586-keV level, the 143 keV, $(M1 + E2)$ transition is used to deduce the widths (with the present assignments no collective $E2$ transition de-excites this level). A partial γ-ray width of $5.6(13) \times 10^{-6}$ eV for the 143-keV γ ray leads to implied strengths of $7.7(29) \times 10^{-7}$ $W.u.$ and $1.5(5) \times 10^{-6}$ $W.u.$ for the 768- and 923-keV transitions, respectively. It should be noted that the above calculations are sensitive to the assumed $K^\pi = 13/2^+$ assignment for the 1433-keV level.

The transition strengths deduced above (of about 10^{-6} W.u.) imply relatively strong transitions once the K-forbiddenness is taken into account. In the rare-earth region, $E1$ transitions with strengths around 10^{-4}-10^{-5} W.u. are expected between certain one-quasiparticle states [52–54] and can be attributed to an enhanced dipole moment due to an octupole softness [55]. However, octupole enhancement is difficult to reconcile with the fairly complex three-quasiparticle to one-quasiparticle configuration changes exhibited in the present case, and the relative enhancement of these $E1$ transitions therefore remains unexplained.

C. Mixing of $15/2^-$ states in ^{175}Tm

The $15/2^-$ isomer at 947 keV has three decay branches to the $7/2^-$ band (see Fig. 2) that exhibit small reduced hindrances. The 5-keV, $M1$ branch has $f_\nu > 14$, the 164-keV, $M1$ one $f_\nu = 28(1)$, while the 301-keV, $E2$ branch has $f_\nu = 8(1)$.

The γ-ray intensity branching ratio of 0.45(4) for the 301-/164-keV transitions agrees within error with a value of 0.47(13) for the 296-/159-keV in-band transitions from the $15/2^-$ band member at 942 keV. The similarity is a signature [6] that the isomer contains a small amplitude of the lower-K band that results in a collective component in the otherwise forbidden transitions resulting in the observed low hindrances.

Using a method similar to Refs. [6, 49], a mixing amplitude between the two $15/2^-$ states of $\beta = 0.010$ can be deduced from the 301-keV, $E2$ isomer branch. This mixing amplitude, and the measured energy spacing of $\Delta E_{exp} = 5.2$ keV, implies an interaction strength of only V = 53 eV. This is a small interaction in comparison to normal nuclear matrix elements that are typically on the order of tens of keV [57]. However, it is comparable to interaction strengths associated with other cases of chance mixing between high- and low-K states, as discussed by Dracoulis *et al.* [6]. A 0.01% component of the $K^\pi = 7/2^-$ band in the $K^\pi = 15/2^-$ wavefunction is, therefore, sufficient to allow this isomer to decay with the low reduced hindrances observed in the data.

The inferred 5.2-keV transition between the two $15/2^-$ states is presumably also allowed, due to the collective component described above. It represents an unusual in-band decay that connects two states with the same J and can only occur because of the state mixing. The situation is displayed (for a general case) in Fig. 21.

The in-band B($M1$) value for bands with $K \neq 0,\ 1/2$, can be written in terms of the

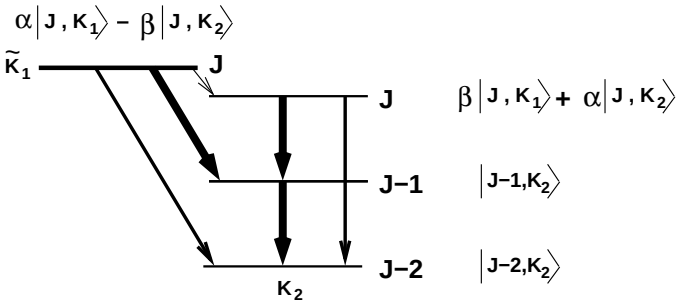

FIG. 21: Mixing of a high-K bandhead with a rotational state of the same spin in a lower-K band. The mixed wavefunctions are shown.

rotational g-factor, g_R, and the intrinsic g-factor, g_K, as [58]

$$B(M1; J_1, K \rightarrow J_2, K) = \frac{3}{4\pi}\,{\mu_N}^2 \times \left[(g_K - g_R) \times K\langle J_1 K 10 \mid J_2 K\rangle + g_R(J_1(J_1+1))^{1/2}\delta(J_1, J_2)\right]^2, \quad (4)$$

where $\mu_N = \frac{e\hbar}{2M_\pi}$ is the nuclear magneton. The last term is only relevant when $J_1 = J_2$, and is, therefore, unphysical in normal circumstances, since two states with the same spin cannot occur in a band.

The $M1$ transition matrix element between two states with spin J, and nominal (mixed) K values, $\tilde{K}_1$ and $\tilde{K}_2$ (see Fig. 21) is given by:

$$\langle J, \tilde{K}_2 \mid T(M1) \mid J, \tilde{K}_1\rangle = \left\langle \beta\langle J, K_1 \mid + \alpha\langle J, K_2 \mid \left| T(M1) \right| \alpha \mid J, K_1\rangle - \beta \mid J, K_2\rangle \right\rangle, \quad (5)$$

where α and β are the wavefunction amplitudes. Neglecting the cross-terms between K_1 and K_2 (i.e., the non-collective components), and rewriting for the present ^{175}Tm case in terms of the experimental B($M1$) value:

$$B(M1; J, \tilde{K}_{15/2} \rightarrow J, \tilde{K}_{7/2}) = \frac{\alpha^2\beta^2}{(2J+1)}\left[\langle J, K_{15/2} \mid T(M1) \mid J, K_{15/2}\rangle - \langle J, K_{7/2} \mid T(M1) \mid J, K_{7/2}\rangle\right]^2. \quad (6)$$

This expression does not look like that for a normal in-band $M1$ transition, but instead takes the form of a difference in the static moments of the two states. By substituting eq. (4) for both right-hand terms in eq. (6), the transition strength for the 5.2-keV transition measured experimentally can be compared with that predicted from the mixing. For simplicity, the same g_R value is assumed for both the $K = 7/2$ and $K = 15/2$ states. The predicted $g_K - g_R = -0.19(8)$ is assumed for the $K^\pi = 15/2^-$ band (whose rotational band is unobserved) along with $g_K - g_R = +0.88(9)$ (from Table VI) for the $K^\pi = 7/2^-$ band. The amplitude $\beta = 0.010$ was deduced earlier, and $\alpha = \sqrt{1-\beta^2}$.

The calculation results in the prediction B($M1$) = $1.8(9)\times10^{-4}\mu_N^2$ for the 5.2-keV transition, which is consistent with the measured limit of B($M1$) $\leq 6.2\times10^{-4}\mu_N^2$. It should be noted, however, that the measured B($M1$) limit is very sensitive to the mixing ratio used in deducing the limit on the 5.2-keV γ-ray intensity.

VIII. SUMMARY

In summary, extensive results on the high-spin structure of odd-A, neutron-rich ^{173}Tm and ^{175}Tm nuclei have been obtained.

In ^{173}Tm, the new states include a three-quasiparticle, $K^\pi = 19/2^-$ isomer with a lifetime of $\tau = 360(100)$ ns at 1906 keV. The level is associated with the $\nu 5/2^-[512]$ $7/2^-[514]\otimes\pi 7/2^-[523]$ configuration. A five-quasiparticle, $K^\pi = 35/2^-$ isomer with a lifetime of $\tau = 175(40)$ ns has also been observed at 4048 keV. The $35/2^-$ isomer is proposed to be a t-bandhead comprised of the $\nu 7/2^+[633]7/2^-[514]9/2^+[624]5/2^-[512]\otimes\pi 7/2^-[523]$ configuration. It is characterized by anomalously fast decays, possibly due to Coriolis mixing within the configuration and to state mixing with nearby levels.

In ^{175}Tm, a candidate for the $9/2^-[514]$ orbital has been identified at 1175 keV. High-K structures in ^{175}Tm include a $K^\pi = 15/2^-$ isomer with a lifetime of $\tau = 64(3)$ ns at 947 keV. The isomer has been assigned to the $\nu 7/2^-[514]$ $9/2^+[624]\otimes\pi{-}1/2^+[411]$ configuration. It shows relatively enhanced decays that can be explained by chance mixing with the $15/2^-$ member of the $7/2^-[523]$ band at 942 keV with a mixing matrix element of only 53 eV. Another isomer with $K^\pi = 23/2^+$ and a lifetime of $\tau = 30(20)$ μs, was observed at 1518 keV. It is proposed to be associated with the $\nu 7/2^-[514]$ $9/2^+[624]\otimes\pi 7/2^-[523]$ configuration.

Multi-quasiparticle calculations were performed for both nuclei, the results of which compare well with the experimentally observed high-spin states. The observed multi-quasiparticle structure of both ^{173}Tm and ^{175}Tm can be understood in terms of the single unpaired proton occupying either the $1/2^+[411]$ or $7/2^-[523]$ Nilsson states with coupling to high-seniority neutron configurations that are observed in the even-even isotones.

Unresolved experimental issues remain nevertheless. In particular, the rotational bands associated with the $35/2^-$ isomer in ^{173}Tm and the $23/2^+$ isomer in ^{175}Tm need to be identified to confirm that the magnetic properties are consistent with the present configuration assignments for the respective states.

Acknowledgments

We are indebted to R. B. Turkentine and J. P. Greene for producing the targets. This work was supported by the ANSTO program for Access to Major Research Facilities,

grant No. 02/03-H-05, the Australian Research Council Discovery projects DP0343027 and DP0345844, and the US Department of Energy, Office of Nuclear Physics, under Contract No. DE-AC02-06CH11357, and Grant No. DE-FG02-94ER40848.

---

[1] G. J. Lane *et al.*, Phys. Rev. C **82**, 051304(R) (2010).

[2] F. G. Kondev, G. D. Dracoulis, A. P. Byrne, T. Kibédi, S. Bayer, Nucl. Phys. A **617**, 91 (1997).

[3] G. D. Dracoulis *et al.*, Phys. Lett. B **635**, 200 (2006).

[4] G. D. Dracoulis *et al.*, Phys. Rev. C **79**, 061303(R) (2009).

[5] G. D. Dracoulis *et al.*, Phys. Rev. C **71**, 044326 (2005).

[6] G. D. Dracoulis *et al.*, Phys. Rev. Lett. **97**, 122501 (2006).

[7] T. R. McGoram, G. D. Dracoulis, T. Kibédi, A. P. Byrne, R. A. Bark, A. M. Baxter, S. M. Mullins, Phys. Rev. C **62**, 031303(R) (2000).

[8] P. M. Walker, *et al.*, Phys. Rev. C **79**, 044321 (2009).

[9] G. D. Dracoulis, *et al.*, Phys. Rev. C **82**, 034317 (2010).

[10] R. O. Hughes, G. J. Lane, G. D. Dracoulis, T. Kibédi, P. Nieminen, H. Watanabe, Phys. Rev. C **77**, 044309 (2008).

[11] C. Wheldon *et al.*, Phys. Lett. B **425**, 239 (1998).

[12] M. Cromaz, T. J. M. Symons, G. J. Lane, I. Y. Lee, R. W. Macleod, Nucl. Instr. Meth. Phys. Res. A **462**, 519 (2001).

[13] D. C. Radford, Nucl. Instr. Meth. Phys. Res. A **361**, 297 (1995).

[14] R. Brun and F. Rademakers, Nucl. Inst. and Meth. in Phys. Res. A **389**, 81 (1997).

[15] T. Kibédi, T. W. Burrows, M. B. Trzhaskovskaya, P. M. Davidson, C. W. Nestor Jr., Nucl. Instr. Meth. Phys. Res. A **589**, 202 (2008).

[16] R. Broda, M. A. Quader, P. J. Daly, R. V. F. Janssens, T. L. Khoo, W. C. Ma, M. W. Drigert, Phys. Lett. B **251**, 245 (1990).

[17] R. Broda, J. Phys. G: Nucl. Part. Phys. **32**, R151 (2006).

[18] R. O. Hughes *et al.*, to be published.

[19] G. Løvhøiden, P. H. Andersen, D. G. Burke, E. R. Flynn, J. W. Sunier, Nucl. Phys. A **327**, 64 (1979).

[20] S. Drissi, A. Bruder, J. Kern, J. P. Vorlet, Nucl. Phys. A **483**, 153 (1988).

[21] X. Zhang, S. Yuan, W. Yang, Z. Li, W. Mou, X. Yu, J. Zhong, Z. Phys. A **353**, 353 (1996).

[22] M. S. Basunia, Nucl. Data. Sheets **102**, 719 (2004).

[23] V. Pursiheimo, T. Tuurnala, T. Raunemaa, Z. Phys. **252**, 283 (1972).

[24] R. W. Tarara, J. D. Zumbro, C. P. Browne, Phys. Rev. C **18**, 1064 (1978).

[25] S. J. Asztalos *et al.*, Phys. Rev. C **60**, 044307 (1999).

[26] N. J. Stone, At. Data and Nucl. Data Tables **90**, 75 (2005).

[27] M. L. Bissell *et al.*, Phys. Lett. B **645**, 330 (2007).

[28] V. S. Shirley, Nucl. Data. Sheets **75**, 377 (1995).

[29] J. Kern and G. L. Struble, Nucl. Phys. A **286**, 371 (1977).

[30] P. Taras, D. Ward, H. R. Andrews, J. S. Geiger, R. L. Graham, W. McLatchie, Nucl. Phys. A **289**, 165 (1977).

[31] E. N. Kaufmann, J. D. Bowman, S. K. Bhattacherjee, Nucl. Phys. A **119**, 417 (1968).

[32] F. G. Kondev, G. D. Dracoulis, A. P. Byrne, T. Kibédi, Nucl. Phys. A **632**, 473 (1998).

[33] A. E. Stuchbery, Nucl. Phys. A **589**, 222 (1995).

[34] K.E.G. Löbner, Phys. Lett. B **26**, 369 (1968).

[35] L.I. Rusinov, Usp. Fiz. Nauk. **73**, 615 (1961).

[36] K.E.G. Löbner, *The Electromagnetic Interaction in Nuclear Spectroscopy*, W. D. Hamilton ed., (North Holland, Amsterdam, 1975), p. 141.

[37] J. Kantele, Phys. Lett. **2**, 293 (1962).

[38] G. D. Dracoulis *et al.*, to be published.

[39] L. Kristensen, M. Jorgensen, O. B. Nielsen, G. Sidenius, Phys. Lett. **8**, 57 (1964).

[40] N. J. Ncapayi, S. M. Mullins, M. Benatar, E. Gueorgueiva, J. J. Lawrie, G. K. Mabala, S. Mukherjhee, S. H. T. Murray, K. P. Mutshena, R. T. Newman, J. F. Sharpey-Schafer, F. D. Smit, P. Vymers, Eur. Phys. Jour. A **26**, 265 (2005).

[41] G. D. Dracoulis *et al.*, Phys. Rev. C **81**, 054313 (2010).

[42] F. S. Stephens, Rev. Mod. Phys. **47**, 43 (1975).

[43] T. Bengtsson and I. Ragnarsson, Nucl. Phys. A **436**, 14 (1985).

[44] P. Möller, J. R. Nix, W. D. Myers, W. J. Swiatecki, At. Data and Nucl. Data Tables **59**, 185 (1995).

[45] W. Nazarewicz, M. A. Riley, J. D. Garrett, Nucl. Phys. A **512**, 61 (1990).

[46] F. G. Kondev, Ph.D. thesis, Australian National University, unpublished (1996).

[47] K. Jain, O. Burglin, G. D. Dracoulis, B. Fabricius, N. Rowley, P. M. Walker, Nucl. Phys. A **591**, 61 (1995).

[48] G. Mukherjee *et al.*, Phys. Rev. C **82**, 054316 (2010).

[49] T. R. Saitoh, N. Saitoh-Hashimoto, G. Sletten, R. A. Bark, G. B. Hagemann, B. Herskind, Phys. Scr. T **88**, 67 (2000).

[50] P. M. Walker, G. D. Dracoulis, A. P. Byrne, B. Fabricius, T. Kibédi, A. E. Stuchbery, Phys. Rev. Lett. **67**, 433 (1991).

[51] P. M. Walker *et al.*, Nucl. Phys. A **568**, 397 (1994).

[52] F. M. Bernthal and J. O. Rasmussen, Nucl. Phys. A **101**, 513 (1967).

[53] S. Ogaza, J. Kownacki, M. P. Carpenter, J. Gascon, G. B. Hagemann, Y. Iwata, H. J. Jensen, T. Komatsubara, J. Nyberg, G. Sletten, P. O. Tjøm, W. Waluś, I. Hamamoto, Nucl. Phys. A **559**, 100 (1993).

[54] G. B. Hagemann, I. Hamamoto, W. Satuła, Phys. Rev. C **47**, 2008 (1993).

[55] W. Donner and W. Greiner, Z. Phys. A **197**, 440 (1966).

[56] F. P. Cranston Jr., M. E. Bunker, J. W. Starner, Phys. Rev. **110**, 1427 (1958).

[57] G. B. Hagemann *et al.*, Nucl. Phys. A **618**, 199 (1997).

[58] A. Bohr and B. R. Mottelson, *Nuclear Structure*, Vol. II (Benjamin, New York, 1975).